SYNTHESIS, CHARACTERIZATION AND PHOTOCATALYTIC APPLICATION OF MESOPOROUS METALLOSILICATES

A THESIS

SUBMITTED TO THE

UNIVERSITY OF PUNE

FOR THE DEGREE OF

MASTER OF SCIENCE (M.Sc)

(PARTLY BY PAPER AND PARTLY BY RESEAERCH)

IN

CHEMISTRY

BY

ANUJA A. BELHEKAR

PUNE 411008

INDIA

APRIL 2007

CERTIFICATE

Certified that the work incorporated in the thesis "SYNTHESIS, CHARACTERIZATION AND PHOTOCATALYTIC APPLICATION OF MESOPOROUS METALLOSILICATES" submitted by Anuja A. Belhekar for the Degree of MASTER OF SCIENCE (M.Sc) (PARTLY BY PAPER AND PARTLY BY RESEAERCH) was carried out by the candidate under my supervision at Catalysis Division, National Chemical Laboratory, Pune 411 008, India.

Dr. RAJIV KUMAR
(Research Guide)

ACKNOWLEDGEMENTS

I take this opportunity to express my sincere appreciation and deep sense of gratitude to my guide, Dr. Rajiv Kumar, HOD, Catalysis Division, National Chemical Laboratory, for suggesting me this problem and for invaluable guidance throughout this work. I am also thankful to him for providing me all facilities and assistance for carrying out the research work.

I also wish to acknowledge sincerely the cooperation and timely help given by Dr.(Mrs) A.A. Belhekar and Dr. (Ms) S.V. Awate . I would like to express my infinite gratitude to Dr. N.M. Gupta, Emeritus Scientist, Catalysis Division, National Chemical Laboratory for giving me suggestions and encouragement throughout my work.

I am also thankful to Dr. P.N. Joshi, Mr. Tejas Gaydhankar, Miss. Violet Samuel, Mrs. Nalini Jacob, Mr. R.K. Jha, Dr (Mrs) K.R. Kamble and Dr. (Ms) Shubhangi Umbarkar for their help and cooperation for completing this work.

My thanks are due to Director, Dr. S. Sivaram, National Chemical Laboratory, Pune, for allowing me to do this work in Catalysis Division, NCL, Pune.

I am deeply indebted to the Controller, CQA(ME), Pune, for granting me permission to work in National Chemical Laboratory, Pune without which it was not possible to complete the work. I am also grateful to my colleagues in CQA(ME) for their support and encouragement.

Anuja A. Belhekar

LIST OF FIGURES

CONTENTS

INTRODUCTION

1.1. General Introduction

In chemical reactions bonds between certain atoms are broken and others are formed. There are many possibilities for this to give large number of products .However in biological systems as well as in mass transformations performed by man, certain single products are desired. This aim is achieved by the presence of a further substance, a catalyst within the reactive system. Berzelius defined a catalyst as a substance which by its mere presence evokes chemical actions which would not take place in its absence. Catalyst is a substance which did not itself alter during the course of reaction. According to Ostwald, the phenomenon catalysis can be understood as an acceleration of a thermodynamically feasible reaction through the presence of a substance the catalyst; which itself is either essentially altered or consumed by this chemical action. The active site theory suggested by Taylor in 1925 postulates that distinct sites on a catalytic surface can interact with the reactants; he also expressed a view that the amount of surface which is catalytically active is determined by the reaction itself. Catalysts are conveniently divided into two groups – Homogeneous catalysts and Heterogeneous catalysts.

A catalyst is named homogeneous, when the catalyst and reactant are in the same phase, i.e. either in gaseous or in liquid phase. The advantages of homogeneous catalyst lies in the fact that every catalyst molecule becomes accessible to the reactant, since it dissolves in a liquid phase and so catalysis is more efficient. Homogeneous catalysts have several disadvantages if applied in the industrial processes such as wasting large amount of catalysts, corrosion of reactors, water pollution by acidic waste water and difficulties of catalyst recovery [1].

The use of heterogeneous catalysts helped scientists for overcoming the practical difficulties when using homogeneous catalysts. Heterogeneous catalysts are essential for the production and consumption of fuels, manufacture of chemical feed stocks and plastics. Proper channel geometry and pore size distribution are necessary to provide the catalyst with the appropriate sites and site accessibility for the desired activity, selectivity

and stability. Site accessibility in heterogeneous catalysts is controlled by the catalyst pore sizes.

1.2. Mesoporous materials

In 1990, Yanagisawa et al. described the preparation of mesoporous silicas with uniform pore size. Mesoporous materials have attracted considerable attention after the discovery of M41S family of mesoporous silicates because of their controllable pore size, narrow conventionally used zeolites is that the organic molecules with diameter > 10Å can be used for reactions. The porous solid materials are classified as a function of pore diameter[2].

a) Microporous materials [d < 20Å]

b) Mesoporous materials [20 < d<500 Å]

c)Macroporous materials [d > 500 Å]

1.3. Ordered mesoporous silica materials

Constructing solids with expected porous texture and architecture is one of the challenging tasks for researchers all over the world, as the apt design of a porous material can well tune the selectivity for a desired product in a specified reaction. The advent of supramolecular chemistry has given a new thrust to this field of porous solids by the announcement of the formation of mesoporous silicate and aluminosilicate molecular sieves with liquid crystal templates by the researchers at Mobil Research and Development Corporation in 1992 [3,4]. This family of materials generally called M41S molecular sieves consists of one-dimensional hexagonal MCM-41, three-dimensional cubic MCM-48 and lamellar MCM-50. These mesoporous materials with well defined pore sizes of 15 – 100 Å**,** and higher surface areas (>1000 m^2/g) break pastthe pore size constraint (15Å) of microporous zeolites. The synthesis of M41S materials thus paves an explosion of new investigations in the synthesis procedures, synthesis mechanisms, heteroatom insertion, characterization, adsorption and in catalytic reactions [3-7].

1.4. Mechanisms of mesostructure formation

In order to explain the formation of mesoporous materials and in order to provide a rational basis for the various synthesis routes a number of models have been proposed. These models are predicted upon the presence of surfactants in a solution to guide the formation of the solubilized inorganic precursors. Surfactants contain a hydrophilic head group and a long hydrophobic tail group within the same molecule and self organize in such a way as to minimize contact between incompatible ends. The type of interaction between surfactant and inorganic precursor results in various synthesis routes, formation models and the resulting classes of mesoporous materials.

1.4.1. Liquid Crystal Templating Mechanism

A liquid crystal templating (LCT) mechanism was proposed by the Mobil researchers, based on the similarity between liquid crystalline surfactant assemblies [10,11] (i.e. lyotropic phase) and M41S [4]. The mesoporous structure depends upon the length of the hydrocarbon chain, surfactant head group, the effect of variation of surfactant concentration and the influence of organic swelling agents. At low concentration, the surfactant molecules exist as randomly dispersed mono molecules in aqueous solution. With increasing concentration surfactant molecules aggregates with their hydrophobic tails together exposing their polar heads to aqueous solution to reach minimum energy configurations. The lowest concentration at which surfactant molecules aggregate to form spherical isotropic micelle is called critical micelle concentration (CMC-1). Further increase in surfactant concentration initiates aggregation of spherical into cylindrical or rod like micelles (CMC-2). Among the three crystalline phases of M41S materials, the hexagonal phase is the result of packing of cylindrical micelles, the lameller phase corresponds to formation of surfactant bilayers and cubic phase may be regarded as bicontinuous structure.

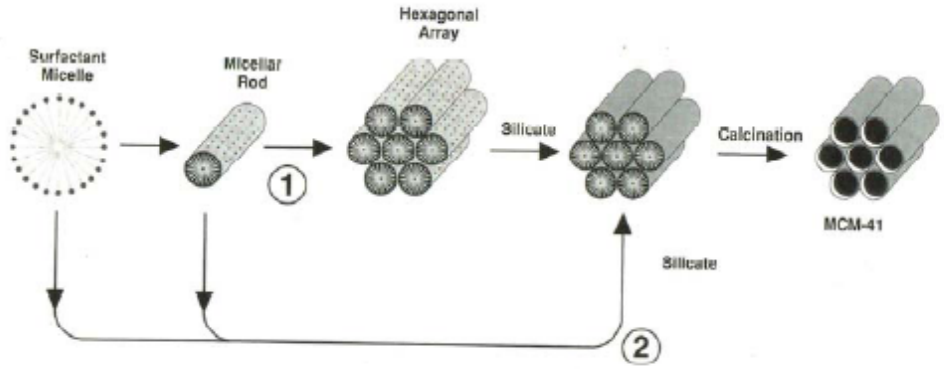

Scheme 1

i) The structure is defined by the organization of surfactant molecules into liquid crystals, which serve as template for the formation of the MCM-41 structure. The first step in the synthesis would correspond to the formation of micellar rod around the rod like structures that in a step would produce hexagonal array of rods, followed by the incorporation of inorganic array around the rod like structures.

ii) The inorganic species mediated, in some manner, the ordering of the surfactants into the hexagonal arrangement.

In either case, the inorganic components that are negatively charged at high pH conditions, interacts strongly with cationic surfactants and the subsequent condensation followed by polymerization leads to mesostructure. However pathway 1

did not take place because the surfactant concentrations used were far below critical micelle concentration (CMC2) required for hexagonal LC formation [12].

1.4.2. Silicate Rod Assembly

Davis et al. [13] by carrying out in situ ^{14}N NMR spectroscopy, found that the LC phase is not present in the synthesis medium during the formation of MCM-41. They proposed that under synthesis conditions suggested by Mobil for the formation of MCM-41 randomly ordered rod like micelle interact with silicate species to yield two or three

layers of silica around the external surface of micelle to yield tubular silica deposited micelle rods. The silicate encapsulated rods, which are randomly ordered, pack to hexagonal mesostructure. Heating and aging complete the condensation of silicate into the as synthesized MCM-41 structure. (Scheme 2)

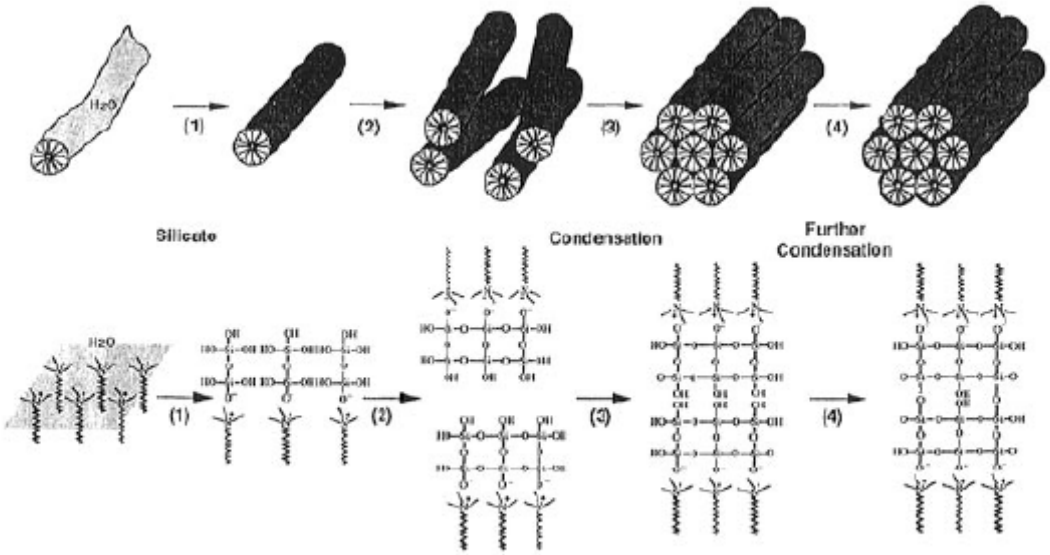

Scheme 2

1.4.3. Silicate Layered Intermediate

Steel et al. [14] postulated that surfactant molecules assembled directly into the hexagonal LC phase upon the addition of the silicate species based on ^{14}N NMR spectroscopy, instead of the formation of silicate covered micellar rods. The silicates were ordered into layers, with rows of cylindrical rods interacted between the layers. Aging the mixture caused the layers to pucker and collapse around the rods, which results in hexagonal phase. Monnier et al. [15] and Stucky et al. [16] postulated a charge density matching model and they suggested that MCM-41 can be derived from a lamellar phase. This is a three-step mechanism. In the first step, the oligomeric silicate polymers act as multidentate ligand for the cationic surfactant head groups leading to strongly interacted surfactant – silica interface with the lamellar phase. In the second step preferential

polymerization of silicate occurs at the interface, so that charge density was reduced. To maintain charge density balance with surfactant head groups, curvature was introduced into the layers, which transformed the lamellar structure into hexagonal structure.

1.4.4. Silicatropic Liquid Crystals

Firouzi et al. [17] found that at low temperature and high pH (~ 14) a true co-operative self assembly of the silicates and the surfactants takes place, in which a lamellar solution of surfactant is transformed into a hexagonal phase in the presence of silicate anions (Scheme 3). Heating of this would lead to the formation of mesostructure materials.

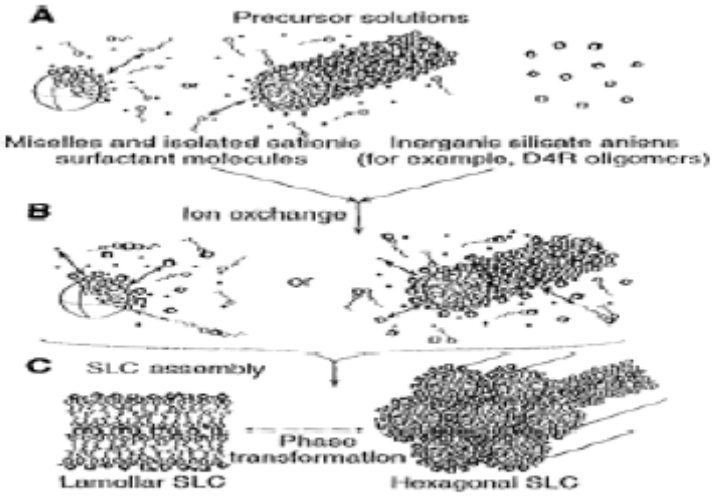

Scheme 3

1.5. Interaction between surfactants and silicate species.

When a silica source is combined with an ionic surfactant like CTMABr in solution the self-organization process involves surfactant /silicate self-assembly and the transformation of mesophase. Scheme 4, shows the aggregation process driven by the silica species and these are very sensitive to pH, temperature, aging time, counter ions and the surfactant species. In the synthesis there are three kinds of charged species in solution: Silica species (I^-/I^+), cationic surfactant (S^+) and its counter ion (X^-). Their

interactions depend on the silicate oligomeric species present because their charge density is different in the degree of oligomerisation. With strong interactions the silicate ions exchange on to the micellar interface and the concentrations results in a rapid condensation of the silicate species.

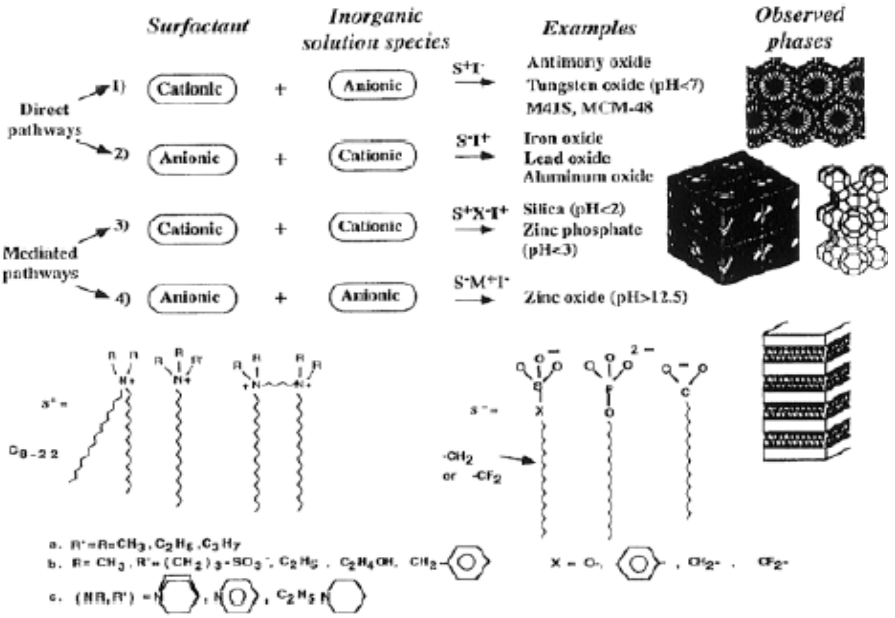

Scheme 4

1.5.1. Changes in acidity with polymerization

The hydrolysis and condensation rate of the silica species are pH dependant. If the pH is lower than the isoelectric point of silica, then the condensation is acid catalyzed and becomes faster as the pH decreases [18]At pH >2 the condensation rate increases with pH until 8 and then decreases again. In a specially designed alkaline synthesis of MCM 41 the initial pH of silicate solution is fairly high (pH=11-12) which leads to highly charged anionic silicate species in solution and a lower rate of condensation. It has the advantage of separating silicate-surfactant (SS) assembly and silica condensation. The initially

homogeneous SS solution can phase- separate into a lyotropic crystalline phase, which leads to different hierarchical structures. This is possible because of the low extent of silica condensation in the surfactant-silicate assembly. After the structure is formed, "delayed way of neutralization" brings down the pH in the range of 8 without the formation of any amorphous silica phase. The lower pH leads to further silica condensation and thus leads to mesoporous materials with thicker walls [19]. Indeed the pH is low enough; otherwise calcinations of the materials may cause a collapse in the mesostructure [20].

1.5.2. Alkaline synthesis of mesoporous silica

In alkaline surfactant-silicate assembly equilibrium can be shifted by the presence of other ionic species in solution. This mean that the salt can effect the screening of the surfactant charge and hence the structure of the assembly. In the synthesis mixture, silicate polymerization can occur either at the surfactant/water interface or in the solution. The competition with the X^- anions to bind with micelles depends on the relative binding ability of silicate anion species with respect to counter ion. Xios et al., [21] made mesoporous silica with hexagonal structure possessing high acidity and hydrothermal stability. They used TEAOH to separately develop a zeolytic nanocluster as silica precursor to make the mesoporous materials with cationic surfactant.

1.5.3. Acidic synthesis of mesoporous silica

In acidic media (pH < 2), the positively charged silica oligomers cannot combine directly with positive surfactant and for charge balance, there must exist a bridge conterion (X^-) at the interface of silicas and surfactants. In acidic synthesis, the silica is usually less condensed and the structure order is thus softer and often leads to rich morphologies (such as film, fiber, and gyroid) [22, 23]. In acidic synthesis one can involve the surfactant mesophase first and then use the structure as a template. Because of the weaker

surfactant-silicate interaction the original liquid crystalline phase can be preserved when mixing with silica sources.

1.6. Modification of Mesoporous Material

The mesoporous material is modified by wet impregnation method at post synthesis step. Post-synthesis treatment will primarily modify the wall surface and thus lead to an increased concentration of the heteroelement on the surface. MCM-41 is loaded with Ti using titanium isopropoxide in isopropanol (Si / Ti =10) since semiconductor photocatalysis will degrade the volatile organic compounds into CO_2 and H_2O and doped with either Au or Cr using chloroauric acid or $CrCl_3$ respectively to increase the life of electron-hole pair.

1.7. Photocatalysis

TiO_2 exhibits three distinct polymorphs (anatase, rutile and brookite) of which only anatase is functional as a photocatalyst. Anatase is a typical n-type semiconductor with a band gap of 3.2 ev. Applications of photocatalysis, (catalysis under light irradiation) have increased these days. Semiconductor photo catalysis with primary focus on TiO_2 as durable photo catalyst has been applied to a variety of problems of water and air purification. It has been useful for

1. The destruction of microorganisms such as bacteria and viruses
2. The inactivation of cancer cells
3. To control odor
4. The photo splitting of water to produce hydrogen gas.
5. The fixation of nitrogen and for cleans up of oil spills
6. The air in fruit, vegetables and cut flower storage area to prevent spoilage and to increase the product shelf life.

The primary criteria for good semiconductor photo catalysts for organic compound degradation are that the redox potential of the $H_2O/OH\bullet$ couple lies within the band gap

domain of the material and that they are stable over prolonged period of time. Semiconductors (e.g. TiO_2, ZnO, Fe_2O_3, CdS, and ZnS) can act as sensitizer for light – reduced redox processes due to their electronic structure, which is characterized by a filled valence band and empty conduction band. Titanium is biologically and chemically inert; it is stable with respect to photo corrosion and chemical corrosion, and is inexpensive also.

TiO_2 has band gap 3.2eV and can absorb UV radiation only. So there are limitations for the use of TiO_2 for the use of environmental remediation of pollutants from practical point of view. TiO_2 can make use of only 3-5% of UV solar radiation reaching the earth. The artificial UV source is expensive due to use of high power supply. To make use of maximum (~95%) visible solar light reaching the earth, the need to have the photocatalyst active in visible light is of prime importance.

Different semiconductors active in visible light such as CdS, ZnO, Fe_2O_3, and ZnS etc are reported [24] till today, but have their own merits and demerits in visible light. When TiO_2 is substituted by transition metals like Fe, V, Cr, their absorption edges shift in the visible light [25]. These anchored transition metal oxide species exist in highly dispersed tetrahedral co-ordination state and act as efficient photocatalyst for various photocatalytic reactions such as decomposition of NO into N_2+O_2. Charge transfer excited state of these transition metal oxides (Ti^{3+} -O^-), (V^{4+}-O^-) play a vital role in the photoreactions of these oxide species. In VIS spectra their absorption edges are in the vicinity of 500-600 nm, thus shifting the band gap position to about 2.0eV. These catalysts show photochemical reactions in the visible light. Karakitsou and Verykios reported [24] that doping TiO_2 with cations of higher valency than that of Ti (IV) resulted in enhanced photoreactivity. They have also noted that doping with trivalent and pentavalent cations was actually detrimental to the photoreactivity of TiO_2.

Recently, by applying an advanced metal-ion-implantation method by bombarding TiO_2 with high-energy metal ions, electronic properties of the TiO_2 are reported [26]. The volatile organic compounds (VOCs) are widely used in industrial processes and domestic activities. These extensive uses lead to water and air pollution, particularly in indoor air pollution. Many VOCs are known to be toxic and considered to be carcinogenic. Photo

catalytic degradation of organic compounds using TiO_2 as a catalyst has been proposed as an alternative advanced oxidation process (AOP) for the decontamination of water and air. Air emission from many industrial sources and remediation sites contain chlorinated volatile organic compounds that require treatment before being released in the environment. Dye pollutants from the textile industry and photographic industry are the main source of environmental contamination. These wastewaters are highly colored and resistant to microbial degradation. They get converted into toxic compounds. The photo degradation of several dye molecules in aqueous TiO_2 suspension with ultraviolet radiation has been reported.

Advanced oxidation process is initiated from the generation of electron-hole pairs on the semiconductor upon absorbing ultra-violet light with the energy equal to or higher than the band gap energy. Electrons and holes generated in the bulk of the semiconductor move to the particle surface. Electrons reduce electron acceptors such as molecular oxygen, and holes can oxidize electron donors including adsorbed water or hydroxide anion giving hydroxyl radical. Many classes of VOCs such as halogenated hydrocarbons; ketones, alcohols, aldehyde and aromatic compounds have been widely used in industries.

There are two types of pollutants

1. Primary pollutants-Directly emitted by a source. eg. NOx, ($NO+NO_2$) and SO_2
2. Secondary pollutants- Formed in the atmosphere through secondary reactions eg. Ozone, Formaldehyde and acetaldehyde etc.

Osaka University has implanted a field using TiO_2 as a photocatalyst since 1996. Photocatalysis should be applied for general roads in urban area with heavy transportation. In Japan application of photocatalysis is expanding for roads to prevent pollution.

Pollution is the global problem, which is increasing day by day due to the large uncontrolled population and problems arising out of it. The exhaust gas coming from vehicle and industries pollutes air as well as water to the vital extent. Need of safe and clean chemical technologies to overcome these problems is necessary. Photocatalysis is one of such systems, which operates at room temperature and is being used for

purification of polluted water and decomposition of toxic chemicals like NOX, chlorofluorocarbon, VOC in the air etc.

Environmental pollution due to volatile organic compounds (VOC) is becoming a serious problem because of inadequate technological solution. Nitro aromatic compounds such as nitrophenol, nitrobenzene, nitrotoluene and nitrobenzoic acid are used in the manufacture of pesticides, dyes and explosives. The industrial solvents and effluents from these industries contain significant level of these pollutants. Wastewater from dye industries contains lot of impurities and so some chemical process is required to degrade these impurities.

Due to this semiconductor catalyst, organic compounds are mineralized to CO_2 and H_2O in presence of UV radiation. This is called optical solid surface or interface reaction. Titanium dioxide absorbs UV rays, and electrons and holes are generated inside it. Electron and holes near the surface are involved in reaction. The generation of many electrons and holes leads to higher reaction effect. The generated holes have strong oxidizibility, and generate hydroxyl radicals by reacting with at the surface of titanium dioxide. The generated hydroxyl radicals have strong oxidizability and cause oxidative reactions with organic compounds. In the presence of oxygen, radicals of the intermediates of organic compounds and oxygen molecules induce a radical chain reaction and consume oxygen. In presence of O_2 and H_2O e^- react with O_2 to form O_2^- and h^+ with H_2O to form OH? radicals. They have high oxidation potential inducing complete oxidation reaction to form CO_2 and H_2O.

Heterogenous photocatalysis is one of the techniques used for this purpose. The basic principle of heterogeneous photocatalysis where semiconductor material is used can be summarized as follows:

A semiconductor is characterized by an electronic band structure in which highest occupied energy band is called valence band (vb) and the lowest empty band is called conduction band (cb), which are separated, by a band gap. When a photon of energy higher or equal to the band gap is absorbed by semiconductor particle, an electron from valence band is promoted to cb with simultaneous generation of hole in the vb.

TiO_2 photocatalysis has been improved by numerous investigations in recent years, particularly owing to its application for complete mineralization of almost all organic contaminants into CO_2 and H_2O. The low rate of electron transfer to oxygen and high recombination rate of electron-hole pairs limits the rate of photo-oxidation of organic compounds on the surface of a catalyst. The noble metals of gold and platinum were usually used to produce the highest Schotty barrier among the metals to facilitate the electron capture.

The oxidative degradation of volatile organic contaminants via photocatalytic route is found to be a practical and cost effective means for controlling of the environmental pollution. Concerted research has therefore been devoted to this subject over the past few years [28-33]. Nevertheless, the low quantum yield and poor stability of the presently available photocatalytic materials have posed limitations on the large scale application of the above-mentioned process. These deficiencies arise mainly due to the following reasons: i) dependence on UV radiation due to large band gap and therefore difficulty in using a photo-catalyst for economic outdoor requirements, ii) a low rate of electron transfer to reactant molecules including oxygen, and iii) a high rate of recombination of electron-hole pair resulting in low quantum yields. With a view to overcome these constraints, various approaches have been attempted to enhance the efficiency of photocatalytic materials, viz. by bringing out certain structural and morphological modifications or by incorporation of certain co-catalysts. In the case of widely-studied titanium dioxide photocatalyst, following strategies have been adopted: i) change in crystallite size of bulk TiO_2, e.g. by preparing through sol-gel or hydrothermal route or by deposition of a thin film over an appropriate host matrix [28-39], ii) doping of TiO_2 with a group VIII metal or a noble metal such as Au to increase the lifetime of electron-hole pair and extending the light absorption to visible region (40-51], iii) chemical substitution at Ti or O sites, so as to modify the band characteristics and to shift the absorbance towards visible region [50-55] and iv) incorporation of TiO_2 in the framework or in the pore system of certain mesoporous materials in order to increase the exposed area [55-59]. In spite of these recent developments, a practical photocatalyst still eludes us.

Mesoporous materials have attracted considerable attention after the discovery of M41S family of mesoporous silicates [60] because of their controllable pore size, narrow pore size distribution and large surface area. Titanium containing mesoporous materials have higher surface area than pure anatase which makes them more effective.

In the recent studies [52, 53], it is demonstrated that the nanosize (2-10 nm) TiO_2 clusters dispersed in mesoporous MCM-41 silica matrix exhibited a microenvironment that was different from that of the bulk titania. Also, the role of TiO_2 crystallite size in the photocatalytic properties is found to relate mainly to the large surface area and hence to the enhanced number of chemisorption sites, rather than to the changes in electronic properties [53]. Metallizing TiO_2 with Pt or Pd can enhance its photocatalytic activity [61] as they have sufficient quantity of holes in the d band and a very low overpotential.

In the present study, we have reported the preparation, characterization and catalytic evaluation of titania loaded on MCM-41, doped with Cr or Au. . The samples have been characterized for their structural and morphological properties using the techniques of powder X-ray diffraction (XRD), diffuse-reflectance UV-visible spectroscopy, low temperature N_2 adsorption, SEM, TEM and FTIR. Visible and UV radiation-induced vapor-phase photo oxidation of acetone have been adopted as representative test reactions, so as to assess the activity of different catalysts for mineralization of contaminating volatile organic compounds.

Objectives of the present study

? To synthesize and characterize MCM-41 and impregnate with Titanium by sol-gel method and dope with Au or Cr .

? To characterize the samples for their structural and morphological properties using the powder X-ray diffraction (XRD), diffuse-reflectance UV-visible spectroscopy, low temperature N_2 adsorption, SEM, TEM and FTIR.

? To study the photocatalytic activity of the catalysts using Visible and UV radiation-induced vapor-phase photo oxidation of acetone .

? To do the calibration of Acetone, CO_2 and air using gas chromatograph with TCD Detector.

? To compare the photocatalytic activity of the catalysts for degradation of acetone at various concentrations.

EXPERIMENTAL

The performance of the catalyst depends upon the preparation method, its pretreatment conditions, and nature of the precursor materials. Even slight change in preparation method can alter the catalytic properties of the catalysts significantly and hence method of preparation is very crucial to get reproducible results. This chapter deals with detailed description for the synthesis of MCM-41 loaded with Ti and doped with Au or Cr.

2.1. Preparation of the catalyst

Materials used:

1) Fumed silica (Aerosil, Aldrich)
2) Cetyl trimethyl ammonium bromide (CTMABr, 99%, Loba Chemie)
3) Tetramethyl ammonium hydroxide (TMAOH, 25 %, Loba Chemie)
4) Titanium isopropoxide (Aldrich)
5) Chromium chloride.

The synthesis of Si-MCM-41 was carried [62] out using the molar gel composition $1SiO_2$: 0.25 TMAOH: 0.18 CTMABr : 25 H_2O at ambient temp 383 K. 3.560g N-cetyl-N,N,N-trimethyl ammonium bromide (CTABr;Loba chemie, 99.8%) was dissolved in 5 g of distilled water (solution I). 4.945 g of tetra methyl ammonium hydroxide (TMAOH;Loba chemie, 25%) was dissolved in 5 g of distilled water(solution II).3.256 g of fumed silica(Aldrich, 99.8%) was added slowly to solution II with constant stirring for 2h. Then solution I was added to above mixture to get thick gel, which was stirred for 2h. Then 5.237 g of water was added again and the gel was stirred for another half an hour. The gel was then transferred to stainless steel autoclave and kept in an oven at 383 K till fully crystalline material is obtained as checked by XRD. Then the sample was filtered, washed thoroughly with cold water and then with about 50 ml acetone. The material was then dried in an oven at 373 K and calcined stepwise upto 813 K and kept for 4h.

Preparation of titania loaded MCM-41, doped with Cr or Au

To the mixture of titanium isopropoxide (Aldrich) in isopropanol and $CrCl_3$, MCM-41 powder was added under stirring for about 1h at ambient temperature, keeping Si/Ti mole ratio 10 and Cr content around 2%. The solution was allowed to dry at room temperature and then the catalyst was calcined in the range 623-773 K for 4h.
For preparing titania loaded MCM-41 doped with about 0-2 % Au required amount of aqueous chloroauric acid solution was added followed by drying and calcination at an optimized temperature of 623 K .

2.2 Characterization

Various characterization techniques are used in order to understand the physicochemical properties like particle size, pore size and surface area. Various techniques and the information obtained from these is listed:

CHARACTERIZATION TECHNIQUE	: INFORMATION
X-ray Diffraction	: Identification of phase
UV-VIS DRS	: Presence of the transition metal in the different environment
FTIR	: Structural changes due to incorporation of the heteroatom
N2 adsorption – desorption	: Surface area and pore size Distribution
Scanning electron microscopy	: Surface morphology and particle Size
Transmission electron microscopy	: Surface morphology and nanosize particle

2.2.1 X-ray diffraction

The structural properties of the catalysts were examined by powder XRD technique. X-

ray interacts with electron in matter and are scattered by the electron clouds of atoms. The sample is irradiated with monochromatic X-ray light and the stray radiation is recorded.

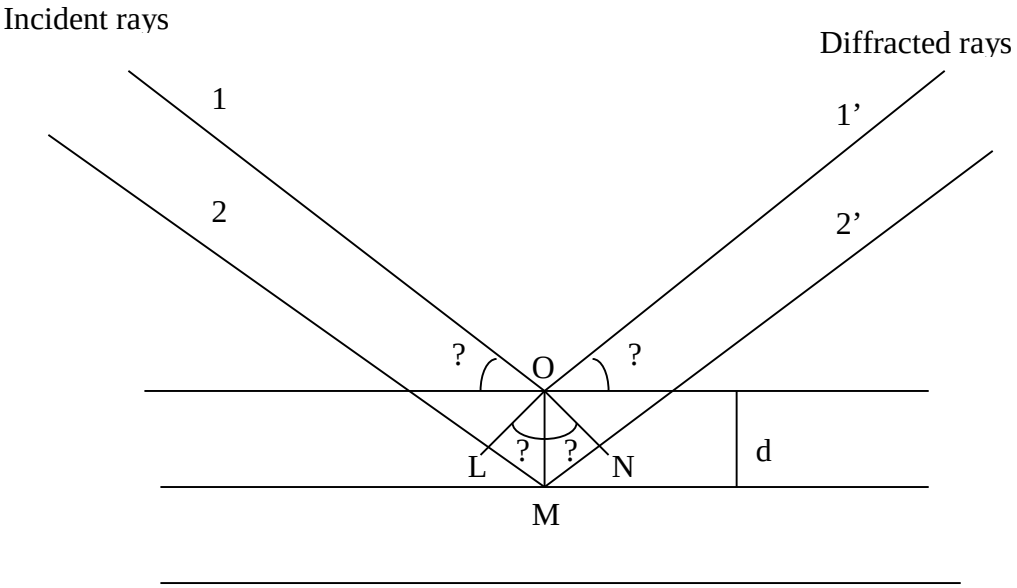

Fig.1: Principle of XRD – Bragg's Equation

Basic principle of X-ray diffraction analysis uses the property of crystal lattice to diffract monochromatic X-ray light. This involves the occurrence of interferences of the waves scattered at the successive planes, which are described by Bragg's equation,

n ? = 2d Sin?

1 & 2 : Incident rays

1'& 2' : Diffracted rays

Path difference = MN + LM

n = order of diffraction.

? = wavelength

d = distance between each set of atomic planes of the crystal lattice,

? = angle of diffraction.

Every atom in a crystal scatters an X-ray beam incident upon it in all directions. Because even the smallest crystal contains very large no. of atoms, the chance that these scattered

waves would constructively interfere would be almost zero except for the atoms in crystals arranged in regular, repeatitive manner. The condition for diffraction of beam of X-ray from a crystal is given by Bragg's equation.

Atoms exactly half way between the planes exert maximum destructive interference, and those at some intermediate location interfere constructively or destructively depending on their exact location but with less than their maximum effect. Thus the position of the diffraction beams from a crystal depends only on the size and shape of the repetitive unit of crystal and the wavelength of the incident X-ray beam, whereas the intensities of the diffracted beams depend on the type of the atoms in the crystal. The diffraction pattern is thus a fingerprint of a crystalline compound and the crystalline components of a mixture can be identified individually.

X-ray tube is a high vacuum, sealed-off unit, usually with copper or molybdenum target. Because the target becomes very hot due to collisions of high-energy electrons, it is cooled by water and is sometimes rotated when a very intense X-ray beam is generated. The X-ray beam passes out of the tube through a thin window of Beryllium or a special glass. Radiation from an X-ray tube is collimated either by a series of closely spaced, parallel metal plates or by a bundle of tubes. The element having an absorption edge at a wavelength between the two similar spectral lines used as a filter to reduce the intensity of the line with the shorter wavelength.

For analytical purposes X – ray radiation may be utilized in several distinct ways .

1. The absorption of X-rays will give information about the absorbing material just as will absorption in another spectral region.
2. The diffraction of X- rays permits analysis of crystalline substance with a high degree of specificity & accuracy.
3. Wavelength measurements will identify elements in sample which is undergoing excitations

DETECTORS

1) Ionization chamber

2) The Geiger counter

3) Proportional counter

4) Scintillation counter.

ADVANTAGES

1) It is a rapid accurate method for identifying the crystalline phases in material

2) It can distinguish isomers, polymorphs (graphite or diamond.), conformers and different hydrated structures.

3) It is a non-destructive analysis for powder samples.

APPLICATION

It is used for determining

1. Lattice parameters
2. Density calculation.
3. Crystallite size.

Crystallite size determination

By using Scherer equation

$L = K.? / ß_{(1/2)} \cos?$

Where

K = Instrumental constant (1 – 0.9).

Cu K_a? = Wave length in Å = 1.5418 Å

T = Angle in degree

$ß_{(1/2)} = 2?_2 - 2?_1$

Powder X-ray diffraction analysis helps to identify the structure, phase purity, degree of crystallinity, unit cell parameter, crystallite size and also the kinetics of crystallization of various molecular sieves. A phase is assumed to be pure when the X-ray pattern matches with that of the reported one and some or all peak positions are differing with those of the reported structures in the case of new structures. A fixed wavelength is chosen for the

incident radiation and the diffraction pattern is obtained by observing the intensity of the scattered radiation as a function of the scattering angle 2? . The d spacing can be found from the Bragg's equation, which relates d spacing and scattering angle with the wavelength of the incident radiation.

The catalysts mentioned above were examined for their structural, optical and photo catalytic properties. In the wide-angle range, powder XRD patterns were recorded on Rigaku, Miniflex (D Max III VC) XRD machine (CuK_{α} radiation) operated at 30 kV and 15 mA.

2.2.2 Surface area measurement

Measurement of surface area of solid catalyst can be done by adsorption using the BET method proposed by Brauner,Emmet and Teller,which assume the dynamic equilibrium between the adsorbed molecules and the molecules in the gas phase. They differ from Langmuir in assuming that the adsorption is multilayer where, the first layer is the truly adsorbed layer and subsequent layers are the condensed ones. The BET plot obtained by volumetric method is generally used for the measurement of the surface area of the catalyst. From the BET equation

$P/V\ (P_o - P) = 1/C\ Vm + (C-1)\ P/C\ Vm\ P_o$

Where, P = adsorption equilibrium pressure

P_o=saturation vapour pressure of the adsorbate

V= volume of nitrogen adsorbed at pressure P

Vm=volume of nitrogen necessary to form a mono layer on unit surface

C = BET constant

A plot of $P/V\ (P_o-P)$ verses P/P_o should give straight line with slope of (C-1)/Vm C and intercept of 1/VmC , from which the monolayer capacity Vm can be calculated. The monolayer volume of the adsorbate converted to NTP is related to the total surface as ,

Total surface = $Vm.N.Am.10^{-20} / 22414(m^2)$

Where N=Avogadro number

Am=the cross sectional area of the adsorbate (for Nitrogen, Am = 16.2A02)

The specific surface (m^2/g) is obtained by dividing total surface by weight (g) of the Sample.The specific surface area , total pore volume and average were measured by N2 Adsorption desorption method using NOVA 1200 (Quanta Chrome) instrument

2.2.3 Scanning Electron Microscope

Basic Principles of SEM

The principle of a scanning electron microscope or SEM functions by scanning a finely focused beam of electrons onto a sample. The impinging electrons interact with the samples molecular composition. The energy of the impinging electrons onto a sample is directly in proportion to the type of electron interaction that is generated from the sample. A series of measurable electron energies can be produced which are analyzed by a sophisticated microprocessor that creates a pseudo three-dimensional image or spectrum of the unique elements that exist in the sample analyzed. It is this series of electrons which are deflected by collisions with the samples electrons.

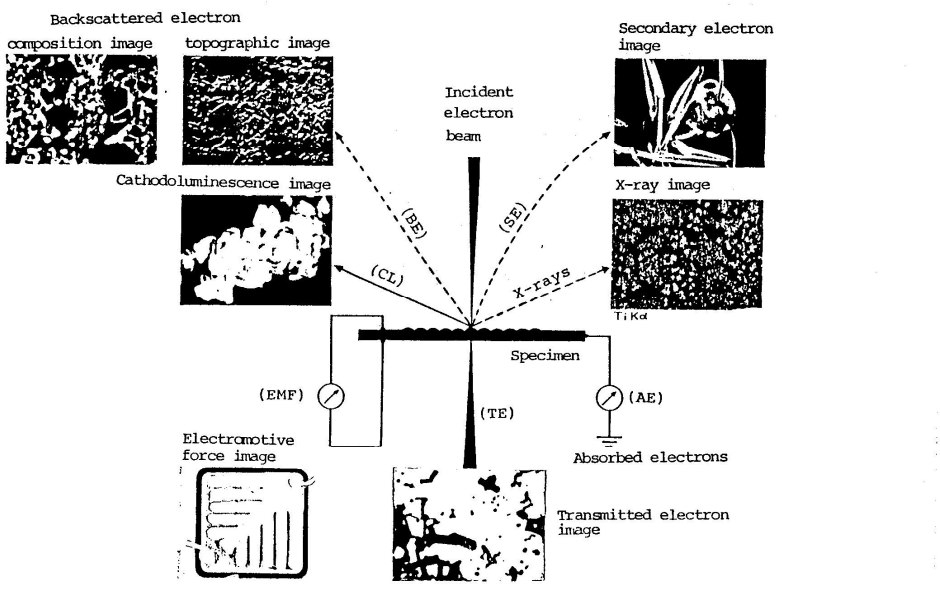

Fig 2: Signals obtained from specimens

Specimen imaging Scanning coils within the SEM serve to scan the electron beam across the sample surface in a 'raster' fashion (as a TV image is built up for example by the fast scanning left-to-right and then downwards of hundreds of lines to give a complete image). When the electron beam hits a specimen a number of different interactions occur with the specimen as shown in Fig.2. These interactions give rise to electron emission from the sample surface. Secondary electrons are used for routine, morphological imaging in the SEM. A secondary electron detector collects them, which very simply comprises a disk of phosphor (where electrons are converted to photons) behind which is a photo multiplier (light tube) through which the signal is transmitted. This light signal is converted to electrons which are subsequently amplified before being used to modulate the intensity of a cathode ray tube display. In this way the image is built up pixel by pixel (the individual 'dots' of information which make up the image) as the beam is scanned across the sample and is then displayed on the display monitor of the PC which controls the SEM instrumentation. The result is a 3-dimensional-looking image of the sample. The block diagram of SEM is shown in Fig.3.

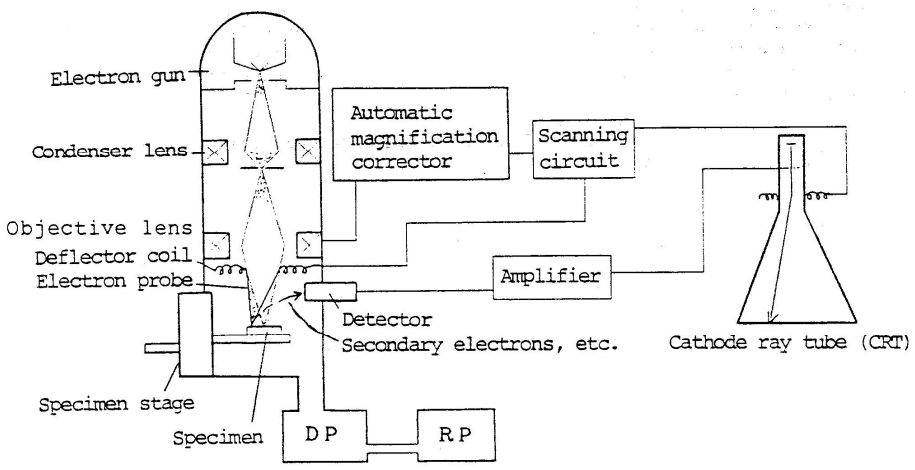

Fig. 3: Composition of Scanning Microscope

SEM is often used purely to visualize detailed surface morphology. Because of its good resolution it may be used at high magnifications (typically 50-100,000X for biological

samples) to reveal fine detail in structure (e.g. hair cells of the inner ear). Relatively low magnification images can also provide a lot of detail.

SEM pictures of the samples under studies are recorded on JEOL-JSM-5200 scanning electron microscope with 5.5 nm resolution, 15KV voltage and 7500x magnification.

2.2.4 Energy Dispersive Spectrometry (EDS)

When the electron beam hits a specimen a number of different interactions (Fig. 2) occur with the specimen; these interactions give rise to electron emission from the sample surface. When an electron is ejected from an inner atomic shell, the result is an ion in an excited state. Through a relaxation process this excited ion gives up energy to return to a normal ground state in the form of electromagnetic radiation –X-rays. The intensity of the characteristic X-rays depends upon the atomic number and a graph of atomic number/ intensity is obtained. We get the concentration of the element in terms of weight % and atomic % calculated from the area of the peak.

Powder sample is loaded on the stub and exposed to electron beam. This is anon destructive technique and very small amount of sample is required.The EDS spectra are recorded on Phoneix EDAX connected to Leica Stereoscan 440 scanning microscope.

2.2.5 Transmission Electron Spectroscopy

Transmission electron microscopy is typically used for high resolution imaging of thin films of a solid sample for micro structural and compositional analysis. The technique involves: (i) irradiation of a very thin sample by a high-energy electron beam,which is diffracted by the lattices of a crystalline or semi crystalline material and propagated along different directions, (ii) imaging and angular distribution analysis of the forward scattered electrons (unlike SEM where secondary electrons are detected) and(iii) energy analysis of the emitted X-rays. In detail, a primary electron beam of high energy and high intensity passes through a condenser to produce parallel rays, which impinge on the sample. As the attenuation of the beam depends on the density and the thickness, the transmitted

electrons forms a two-dimensional projection of the sample mass, which is subsequently magnified by the electron optics to produce the so-called bright field image. The dark field image is obtained from the diffracted electron beams, which are slightly off angle from the transmitted beam. TEM images were obtained on JEOL-2010 CX microscope. Typical operating conditions for TEM instruments are 100-200 keg electrons, 10^{-6} mbar vacuum, 0.5 nm resolutions and a magnification of 10^{5} to 10^{-6}.

2.2.6 UV-Visible Diffuse reflectance spectroscopy

The UV-Visible spectroscopy allows the study of electronic transitions between orbital or bonds in case of atoms, ions or molecules in liquid or solid state. It is known to be a very sensitive and useful technique for the identification and characterization of the metal ion co-ordination and its existence in the framework or extra framework position of metal containing molecular sieves. Electronic transitions are of two types and involve orbital or levels localized in the same metal atoms or adjacent atoms. The first class includes metal centered transitions d-d and (n-1)d-ns (in transition elements),f-f and 4f-5d (in rare earth elements) and ns-nap in the main group elements. The second class involves the charge transfer (CT) transitions from an occupied level centered on a donor atom to a vacant one on an acceptor. This class includes legend to metal and metal to legend charge transfer and transition between MOs in inorganic or organic molecules or ions either free or coordinated to a metal named intra legend charge transfers or legend centered in the later case.

The UV–vies-diffuse reflectance spectroscopy is a suitable technique to study solids, particularly dispersed oxides and metal ions in constrained environment such as M41S, zealots and clay materials to obtain information on the coordination environment, oxidation state of the embedded transition and rare earth metal ions. Diffuse reflectance spectroscopy is a suitable technique for studying heterogeneous catalysts, as both d–d and charge transfer transitions of supported transition metal ions can be probed. Within the past several years, new developments have resulted in a more detailed understanding of the surface chemistry of supported metal oxide catalysts.

Diffuse reflectance (DRS) spectroscopy in the ultraviolet, visible and near-infrared region is, in principle, the most versatile spectroscopic technique, as both d–d and charge transfer (CT) transitions can be probed. One of the advantages of DRS spectroscopy is that the obtained information is directly chemical since the outer shell electrons are probed. Furthermore, the DRS technique can be used under in situ conditions, and is quantitative in nature. The main disadvantage is that diffuse reflectance spectra are complex, and usually encompasses several broad and overlapping bands. To avoid biased spectral analysis, chemo metrical techniques need to be employed.

DRS spectroscopy is a spectroscopic technique based on the reflection of light in the ultraviolet (UV), visible (VIS) and near-infrared (NIR) region by a powdered sample. In a DRS spectrum the ratio of the light scattered from an infinitely thick layer and the scattered light from an ideal non-absorbing reference sample is measured as a function of the wavelength λ. The illumination of powdered samples by incident radiation leads to diffuse illumination of the samples. The incident light is partially absorbed, partially scattered. The scattered radiation, emanating from the sample is collected in an integration sphere and detected. The basic equation for the phenomenological description of diffuse reflection is the radiation transfer equation:

$$\frac{-\mathrm{d}I}{\kappa\rho\,\mathrm{d}S} = I - \frac{j}{\kappa}, \qquad (1)$$

where I is the incident light intensity of a given wavelength; d$a$ds the change of the intensity with the path length ads; ρ the density of the medium; κ an attenuation coefficient corresponding with the total radiation loss due to absorption and scattering; j is the scattering function.

In this theory, the incident and scattered light flux are approximated by two fluxes I and J perpendicular to the surface of the powdered sample, but in the opposite direction. I is the flux of monochromatic diffuse illumination, whereas J is the flux of diffusively scattered light. If the sample is infinitely thick, the diffuse reflection of the sample (R_∞) is related to an apparent absorption (K) and apparent scattering coefficient (S) via the Schuster–Kabala–Monk (S–K–M) or Kabala–Monk (K–M) function:

The samples were further characterized by using UV-Vis diffuse reflectance spectroscopy (Perkins-Elmer, Lambda 650, UV-VIS spectrophotometer). A uniform amount of ~3 wt% of a sample was mixed thoroughly in barium soleplate or neat sample was taken using BaSO4 as standard.

2.2.7 FTIR spectroscopy

Fourier Transform Infrared spectrometers use some form of Michelson interferometer where a beam of radiation is divided into two paths and then recombined introducing a path difference. The two beams interfere and the intensity variation of the beam emerging from the interferometer can be measured as a function of path difference by the detector. The light then enters the Michelson interferometer consisting of the beam splitter (BS), the fixed and the movable mirror and the detector optics: The beam is split up into 2 secondary beams by the beam splitter and the reflected light from the fixed and

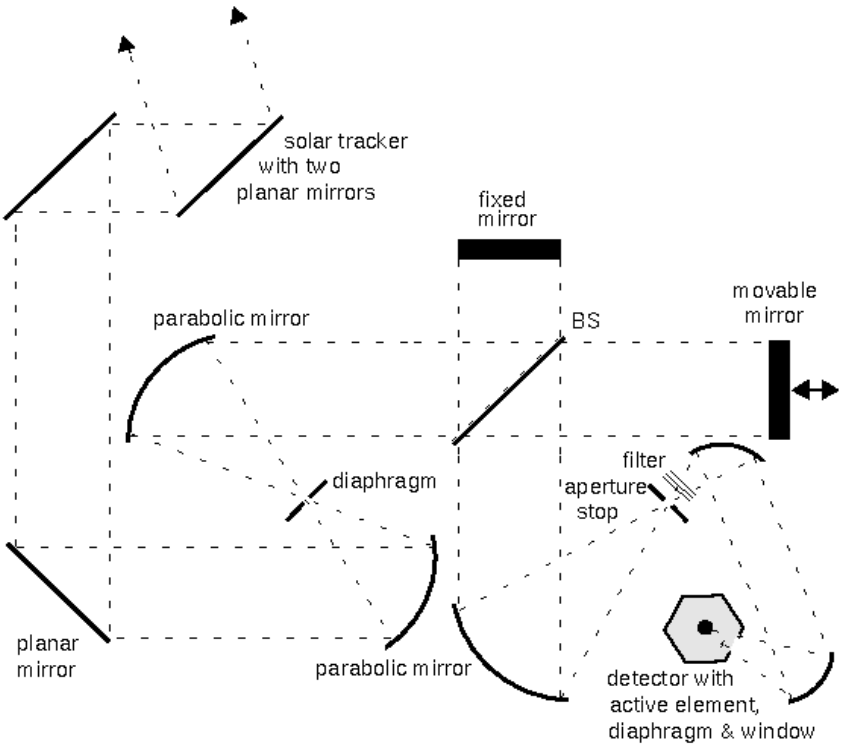

Fig. 4: **Sketch of the FT-IR-spectrometer.**

the movable mirror are recombined at the detector, where an interference pattern as a function of the optical path difference between the two secondary beams is recorded, which is termed the interferogram. The interferogram is converted into a spectrum using the mathematical equation known as Fourier Transform.

Vibrational spectroscopy provides a tool for identifying the surface species of supported catalysts. Dispersion of metal species and its structure, metal-support interaction and metal-metal interactions are some of the valuable information obtained from these studies. The intensities of the IR absorption depends upon the changes in the dipole moment brought by the variation in the molecular geometry. The IR spectra in the framework region (1300-400cm^{-1}) provides information about structural changes while the concentration of hydroxyl region (4000-3000 cm^{-1}) gives a qualitative idea about the strength of acid sites and silanol groups. The acidic and basic properties as well as its strength can also be determined by FTIR spectroscopy using pyridine, NH_3 etc. as the probe molecules.The present FTIR spectra are recorded in nujol matrix using Shimadzu 8300 FTIR spectrometer.

2.2.8 Gas chromatography

Chromatography is the science of separation, which uses a diverse group of methods to separate closely, related components of complex mixtures. During gas chromatographic separation, the sample is transported via an inert gas called the mobile phase. The mobile phase carries the sample through a coiled tubular column where analytes interact with a material called the stationary phase. For separation to occur, the stationary phase must have an affinity for the analytes in the sample mixture. The mobile phase, in contrast with the stationary phase, is inert and does not interact chemically with the analytes. The only function of the mobile phase is to sweep the analyte mixture through the length of the column.

Theory of Operation

The purpose of separation is to allow identification and quantization of individual components of a mixture. In addition to separation, detection of analytes after separation, which is an essential but separate aspect of chromatography, is presented in the section

describing system components. Basic components of a complete gas chromatographic system include: (1) a carrier gas supply, (2) a syringe for sample introduction, (3) the injection port, (4) the column and oven, (5) the detector and data collection system. Before separation occurs in the chromatographic column, the mixture of components in the sample is introduced into the chromatograph through the inject port with a syringe. At this point, the analytes are vaporized (if not already in the gas phase) by the high temperature maintained in the injection port. The analytes are kept in the gaseous state by maintaining all elements of the instrument at a temperature above the boiling point of the analytes. The gas phase analytes are then immediately swept onto the chromatographic column by the mobile phase. The mobile phase comprises of an inert carrier gas. As the analytes are swept through the column by the mobile phase, separation occurs based on the affinity of each analyte for the stationary phase. The gas chromatographic column is composed of a coiled, tubular column and the stationary phase within the tube. GC columns are either packed or open-tubular. In modern open-tubular columns, the stationary phase is a liquid organic compound that is coated on the internal surface of the fused silica column. Components of the mixture with a high degree of affinity for the stationary phase are strongly retained while components with low affinity for the stationary phase migrate rapidly through the column. As a consequence of the differences in mobility due to affinities for the stationary phase, sample components separate into discrete bands that can be qualitatively and quantitatively analyzed.
As individual components of the mixture elute the chromatographic column, the carrier gas to a detector sweeps them. The detector generates a measurable electrical signal, referred to as peaks, that is proportional to the amount of analyte present. Detector response is plotted as a function of the time required for the analyte eluting from the column after injection. The resulting plot is called a chromatogram. Detector response is generally a gaussian shaped curve representative of the concentration distribution of the analyte band as it elutes from the column. The position of the peaks on the time axis may serve to identify the components and the area under the peaks provide a quantitative measure of the amount of each component system components.

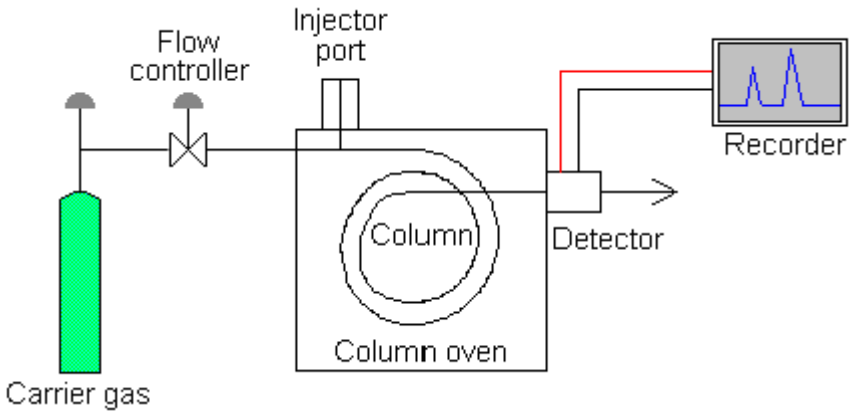

Fig. 5 Schematic diagram of Gas Chromatograph

The primary components of a GC include

(1) Injection port, 2) column, (3) integrator or data acquisition system, (4) detectors **Stationary phase** - An organic liquid compound that is either coated on or covalently bonded to the silica surface of a capillary column. Stationary phases are occasionally solids packed inside the column. The most widely used columns are the fused silica capillary columns due to strength and flexibility. The polarities of the compounds of interest dictate the choice of stationary phase, under the rule "like dissolves like."

Carrier gas - The mobile phase is composed of an inert carrier gas, usually nitrogen, helium, or hydrogen. The choice of carrier gas is frequently determined by the type of detector used and subsequent purity requirements. The sample constituents are transformed into the gaseous phase and are carried along the column during separation. By increasing the speed (flow rate) of the carrier gas, the analysis time can be reduced; however, optimal resolution may be compromised. A faster flow rate also sweeps the injector more efficiently, improving introduction of the sample into the column

Length - Capillary columns vary in length from 15 to 100 meters is a coiled configuration to fit in the instrument oven. For environmental analysis, 30- to 60-meter columns typically are used. Shortening the length of the column can shorten the analysis time; however, resolution (separation) will be compromised.

Diameter - Diameters of open tubular capillary columns are typically between 0.32 and 0.25 millimeter, with high resolution columns having diameters of 0.20 to 0.15 millimeter. The smaller diameter produces better resolution and greater selectivity, but can handle only a small volume of sample (1 to 2 micro liters)

A variety of detectors for gas chromatographs are available. In general, each detector takes advantage of a unique characteristic of a molecule and uses that characteristic to generate a measurable electrical signal.

A flame ionization detector (FID) consists of a stainless steel jet constructed so that carrier gas exiting the column flows through the jet, mixes with hydrogen, and burns at the tip of the jet. Hydrocarbons and other molecules, which ionize in the flame, are attracted to a metal collector electrode located just to the side of the flame. The resulting electron current is amplified by a special electrometer amplifier, which converts very small currents to millivolts. The FID is sensitive to almost all molecules that contain hydrocarbons. Examples include aromatic and chlorinated VOCs, petroleum constituents, SVOCs. The FID is a destructive detector that can be used in series only after nondestructive detectors. The FID is sensitive to water. The FID can detect compounds that contain the low ppb to high part per trillion range.Thermal conductivity detector (TCD) is also used in GC.

Mode of Operation

The majority of GC analyses for environmental applications can be divided into two basic groups: volatile organic chemicals (VOC) and semi-volatile organic chemicals (SVOC). The division is based essentially on the extraction technique used to separate the analyte from the sample matrix. VOC analysis relies on relatively low boiling points and high volatility of the organic chemical. Therefore, the extraction technique frequently is simply heating the sample matrix and driving the analyte into the headspace of the sample container. SVOC analysis, however, requires more sophisticated extraction techniques.

Advantages of FID

1. FID is universal detector and responds to almost any compound that has carbon in it.
2. The response of the detector doesn't change markedly with variation in changes in the flow rate, pressure or temperature of mobile phase and thus provides a very stable detector.

Disadvantages

1. Instruments are complex; they need H_2 and stable environment for the flame.

Applications of Gas chromatography

1. Gas chromatography is used for detection and identification and quantitative estimation of different components in the given reaction mixtures.
2. General trace analysis.
3. Determination of free fatty acids in whole milk.
4. Analysis of tobacco.
5. Food and beverages product.
6. Organic air pollutant.
7. Polyaromatic hydrocarbons
8. Wine flavor and aromas.
9. In biochemical, biomedical and clinical applications.
10. Residual solvent in pharmaceuticals.

The reaction products formed as a function of radiation exposure in the present studies are analyzed with the help of a gas chromatograph (Shimadzu model - R-15A, Porapaq – Q column, TCD detector).

2.3 Catalytic activity

The photocatalytic oxidation of acetone was carried out both under UV radiation (400W mercury vapor lamp with 24000 lumens intensity, UV output 15-20%, range 225-400nm, peak at 365 nm) and also under visible light (halogen lamp, 500W). Both the light

sources were housed in water cooled jackets to cut-off any infrared radiation. 25 mg of a sample was dispersed in a pyrex glass photo-reactor (100 ml capacity) for visible source and quartz reactor for UV source for activity measurement. Different concentrations of acetone vapor in air (1– 25 mole %) were introduced for this purpose after a brief pumping of the reactor. The experiments were conducted under static condition at room temperature, and the reaction products formed as a function of radiation exposure were analyzed with the help of a gas chromatograph (Shimadzu model - R-15A, Porapaq – Q column, TCD detector). The experimental setup is shown in the Fig. 6.

Reaction under visible radiation and under dark condition

No reaction occurred over MCM-Ti and MCM-Ti-Cr (2%) and MCM-Ti-Au (2%) samples, when acetone vapor + air were reacted at room temperature in the absence of radiation. Similarly, no reaction products were formed during the room temperature exposure of these catalysts to acetone or acetone + air in the presence of visible light.

Reaction under UV irradiation

The reaction products formed during photo-oxidation of acetone under UV-irradiation were mainly carbon dioxide and water. The catalytic activity and the yield of these products depended on various factors, such as radiation dose, concentration of acetone in reactant mixture, and the pore characteristics of the catalyst samples. The presence of gold or chromium also resulted in considerable change of the activity of a catalyst, where both the content and the size of the Au or Cr particles played an important role.

The photocatalytic activity was tested for MCM-Ti, MCM-Ti-Au (2%) and MCM-Ti-Cr (2%) for degradation of acetone in acetone + air mixture. First calibration of air was done to calculate unit area of air as mentioned below.

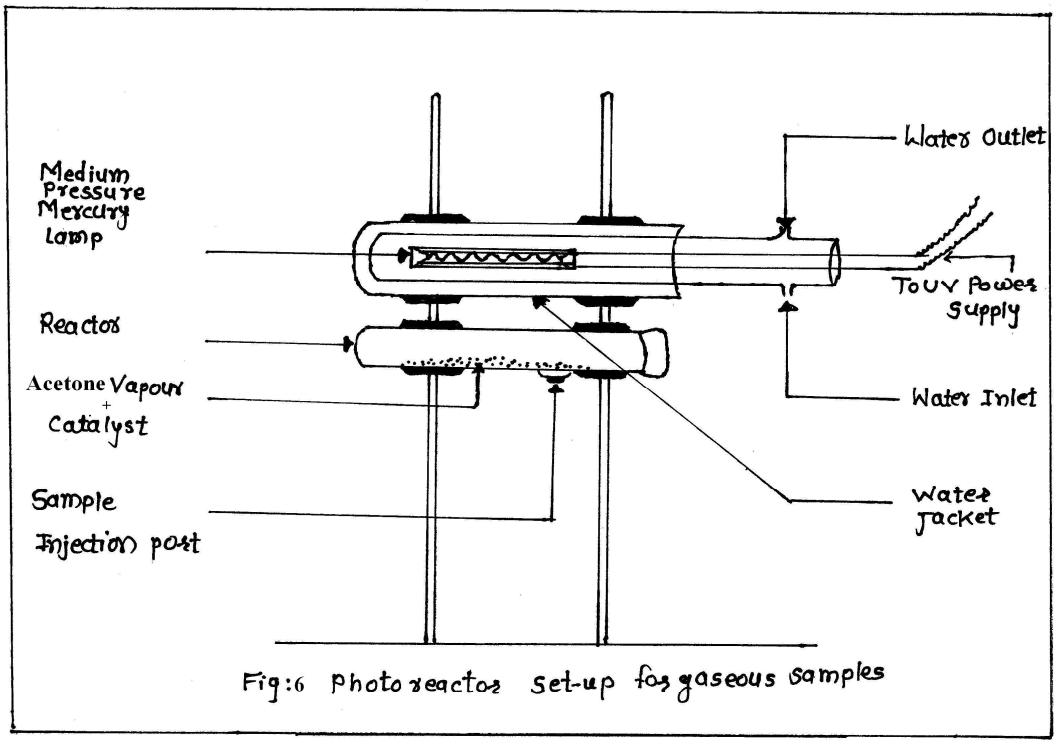

Fig:6 Photoreactor set-up for gaseous samples

Calibration of Air (Att. =3)

Volume (µl)	Area
400	154301
400	151823
200	78309
100	39855
1100	424288

1 unit area of air = 2.593 x 10^{-3} µl

Calibration of CO_2

Volume injected µl	Area of CO_2 (Vol. of CO_2 µl)		Area of air (Volume of air, µl)	
400	165269	367.71	12430	32.23
400	163402	364.91	13532	35.09
200	80077	175.79	9336	24.21
100	43231	85.80	5474	14.19
1100	451979	994.27		

1 unit area of CO_2 = 2.1998 x 10^{-3} µl

Calibration of Acetone

Volume (µl)	Area
1	253754
1	264798
2	479828
2	499904
6l	1498284

1 unit area of acetone = 4.0046x10^{-6} µl

22.4 Litre of CO_2 = 1 mol

1 µl = 0.044642857 µ mol

1 unit area of Acetone = 0.0000040046 µl of acetone

1 unit area of CO_2 = 0.0021998 µl of CO_2

1unit area of air = 0.002593 µl of air

400 µl of mixture of air+acetone was injected in GC and the following chromatograph was obtained showing the peaks due to air, CO_2 and acetone. A typical chromatogram is shown in Fig.7.

It is a graph of intensity vs. time in minutes. The first peak at about 0.46 minutes is due to air. The peak at about 1.8 to 2.00 minutes is due to CO_2 which goes on increasing with time of degradation. The peak at about 14.48 minutes is due to acetone and decreases in intensity as degradation progresses. Thus the peak of CO_2 increases and that of acetone decreases as photodegradation goes ahead and finally all acetone is converted into CO_2 and H_2O.

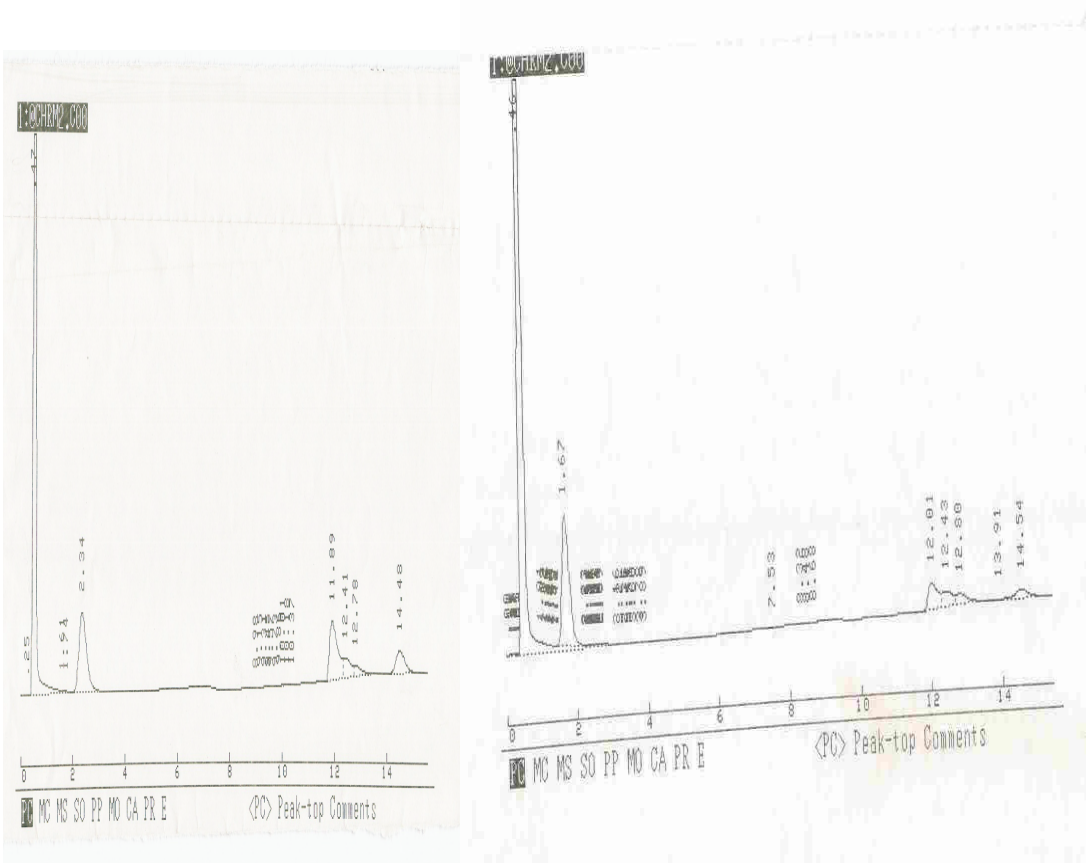

Fig. 7 Chromatogram of MCM-Ti-Au (2%) for degradation of Acetone

RESULTS AND DISCUSSION

This chapter describes the characterization of the synthesized catalysts and their catalytic activity for degradation of acetone at different concentrations. Two sets of samples are prepared namely MCM-Ti-Cr and MCM-Ti-Au keeping Si/Ti ratio ~10 and metal loading (Cr or Au) of 0-2%. The sample designations, structural and textural properties of the samples are listed in Table1

3.1 Description of catalysts

The catalysts prepared are designated as follows:

1) MCM-Ti----MCM-41 loaded with Titanium
2) MCM-Ti-Au (1%) ---MCM-41 loaded with Titanium and doped with 1% gold
3) MCM-Ti-Au (2%)----MCM-41 loaded with Titanium and doped with 2% gold
4) MCM-Ti-Cr (2%)-----MCM-41 loaded with Titanium and doped with 2% chromium

3.2. Characterization of Catalysts

3.2.1 Powder X-ray diffraction (XRD)

Reflection at 2? =25^{o}, 38$^{?}$,48^{o} ,55^{o} and 63^{o} for all the samples in Fig.8 are due to anatase TiO_2. For both MCM-Ti-Au-(1%) and (2%) the increase in the calcination temperature increases the anatase crystallanity. The size of crystallites in different samples, as calculated from the width of I_{112} reflection by using Scherrer's equation, is given in Table 1. The presence of small amount of gold in our samples is indicated by a weak and broad XRD line appearing at 44.5^{o} (d = 2.04 Å) in curves 1-5, revealing the small size of Au crystallites which is absent in curves 6 and 7.The mark * denotes the peaks due to chromium oxide in curve 7.

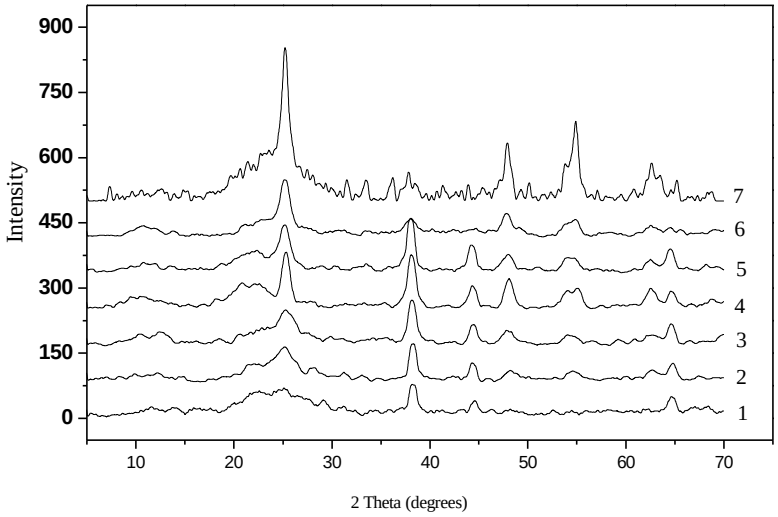

Fig. 8. XRD profiles of (1)MCM-Ti-Au (1%) calcined at 623 K (2) MCM-Ti-Au (1%) calcined at 773 K (3) MCM-Ti-Au (2%) as-synthesized (4) MCM-Ti-Au (2%) calcined at 623 K (5) MCM-Ti-Au (2%) calcined at 773K (6) MCM-Ti calcined at 773 K(7) MCM-Ti-Cr (2%) calcined at 623 K.

Table 1: Structural and textural properties

No	Sample	Calcinations temperature (K)	TiO_2 particle diameter (nm)*	BET specific surface area(m^2/g)+	Total Pore volume (cm^3)	Average pore diameter(Å)
1	MCM-Ti	623	7.1	798	0.6452	32.3
2	MCM-Ti-Au (1%)	623	9.4	549	----	----
3	MCM-Ti-Au (1%)	773	9.7	----	0.3943	31.31
4	MCM-Ti-Au(2%)	623	8.7	531	----	-----
5	MCM-Ti-Au(2%)	773	9.6	----	0.3320	25.01
6	MCM-Ti-Cr (2%)	623	12.2	518	0.4133	24.8

* From XRD data using Scherrer Equation.

+ From N_2 adsorption results.

The figures in bracket ( ) correspond to wt % of Au or Cr

3.2.2 Diffuse Reflectance UV-visible spectra

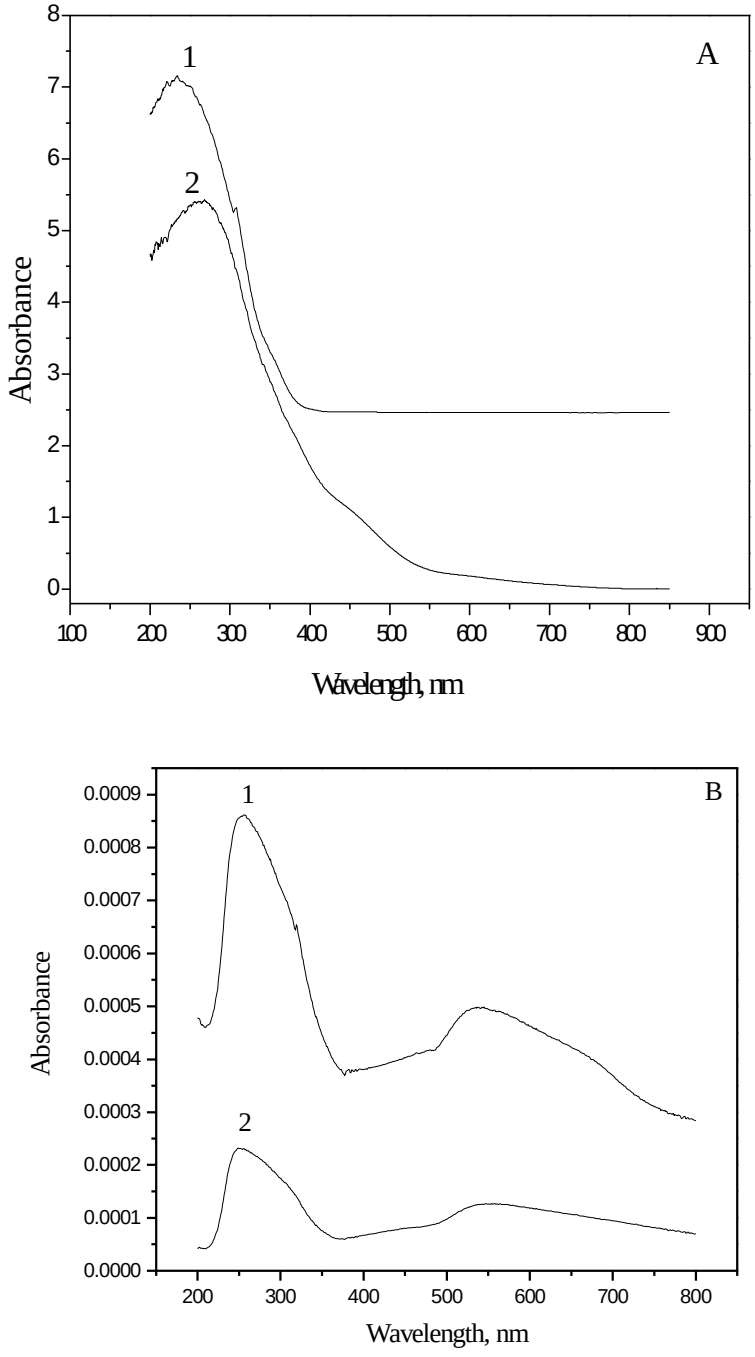

Fig. 9 [A] Diffuse Reflectance UV-vis spectra of MCM-Ti (1) and MCM-Ti-Cr (2%) (2)
[B] Diffuse Reflectance UV-vis spectra of MCM-Au (1%) (1) MCM-Ti-Au (2%)

UV-vis diffuse reflectance spectra of MCM-Ti and MCM-Ti-Cr (2%) are shown in Fig.10A. MCM-Ti without Cr shows no band in the visible region. It resembles to the spectrum of TiO_2 with an absorption band at about 250 nm. MCM-Ti-Cr (2%)shows three absorption edges at ~300, 450 and 550 nm due to the charge transfer O ? Cr and d-d transition in metal oxide respectively [54,63].

UV-vis diffuse reflectance spectra of MCM-Ti-Au (1%) and MCM-Ti-Au (2%) are shown in Fig.10B.Both the samples show a band at 250 nm with less intensity for more gold containing sample. Visible region absorbance at 550-600 nm is a characteristic feature associated with the nano-structured gold arising from d-d transition.

The spectra in Fig.10 A are recorded as neat without adding $BaSO_4$ and those in Fig.10 B are with $BaSO_4$ (3% sample). So the scale on Y-axis is different.

3.2.3 Scanning Electron Microscopy

Fig.10 A and B shows SEM photographs of MCM-Ti-Au (2%) and MCM-Ti-Cr (2%) respectively. The particles in MCM-Ti-Au (2%) are in the range 150-250 nm and in MCM-Ti-Cr (2%) in the range 70-150.

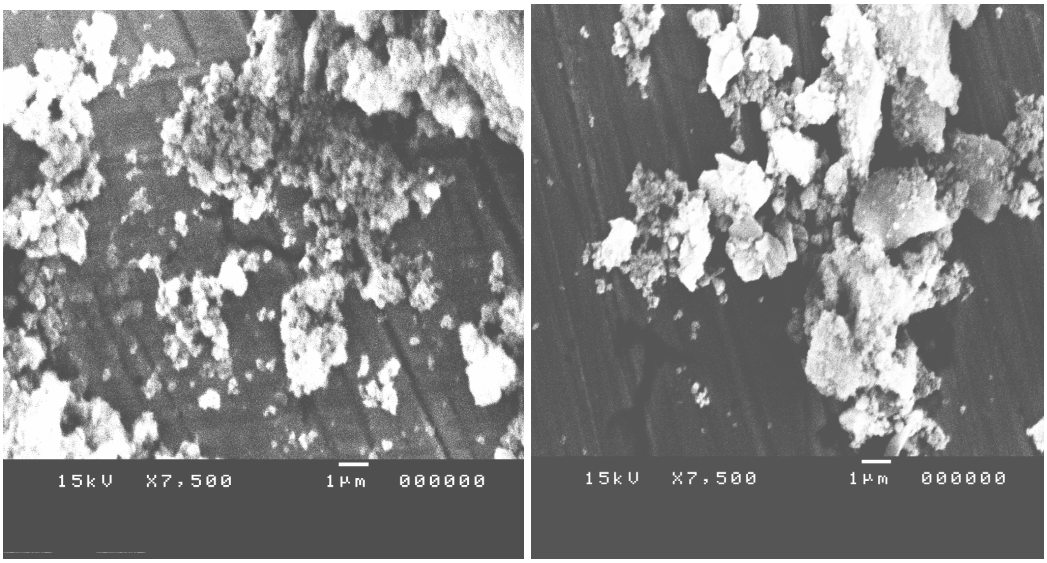

[A] **[B]**

Fig.10: [A] SEM of MCM-Ti-Au (2%) [B] SEM of MCM-Ti-Cr (2%)

3.2.4 Transmission Electron Microscopy

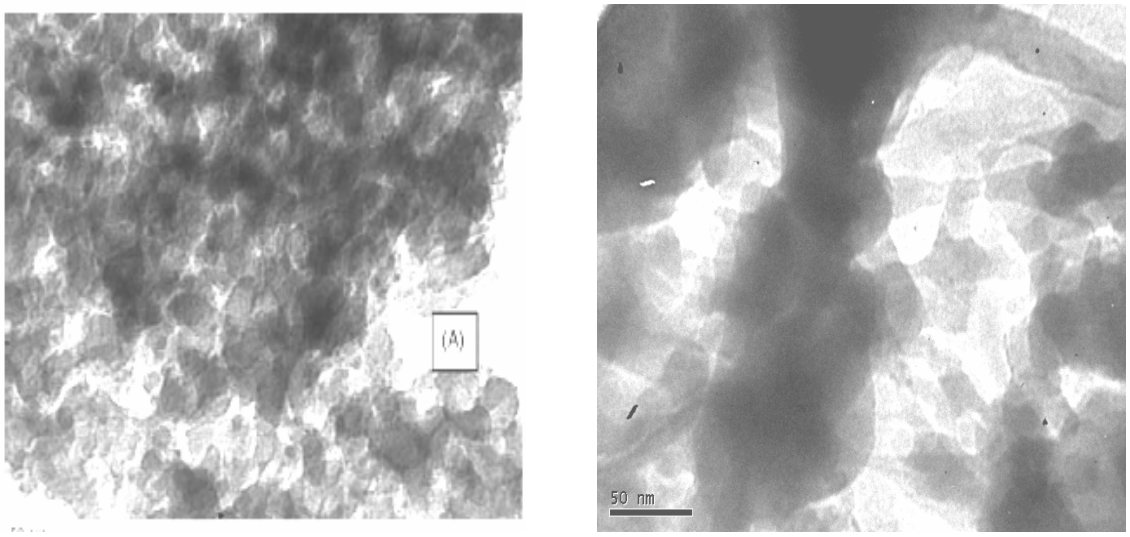

Fig.11 TEM of [A] MCM-Ti-Cr (2%) and [B] MCM-Ti-Au (2%)

Fig 11 A and B show TEM photographs of MCM-Ti-Cr (2%) and MCM-Ti-Au (2%) respectively. Small spots representing TiO_2 has the particle size around 3-4 nm for Cr containing sample and 2-3 nm for Au containing samples. The crystallite size calculated from XRD is 12.2 nm and 9.4 nm for Cr and Au containing samples respectively, which is generally higher than that observed by TEM. This is because TEM shows noncrystalline species which are not detected by XRD.

3.2.5 Nitrogen adsorption study

Adsorption-desorption nitrogen isotherms at 77K on MCM-Ti, MCM-Ti-Cr-(2%), MCM-Ti-Au-(1%) and MCM-Ti-(2%) are shown in Fig 12. The isotherm of MCM-Ti can be classified as type IV according to the IUPAC convention [64] and is typical of mesoporous material. At relative pressure P/P_0 >0.25, a steep rise in N_2 uptake for MCM-Ti is due to capillary condensation inside the mesoporous pores [65] However, Cr or Au loaded samples showed gradual uptake at higher relative pressure. It was observed that

the pore size and BET surface area of the Cr or Au loaded samples decreased compared to the MCM-Ti samples due to blocking of pores. (See Table 1)

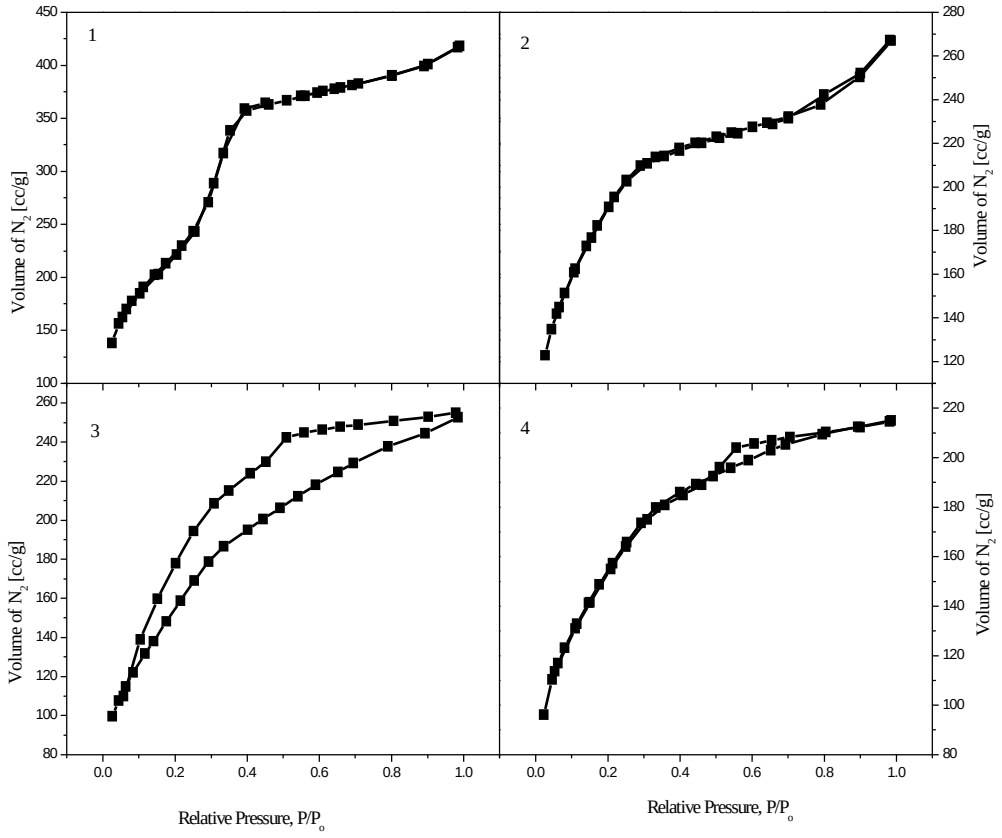

Fig.12. Nitrogen adsorption-desorption isotherms of MCM-Ti (1), MCM-Ti-Cr-(2%) (2), MCM-Ti-Au-(1%) (3) and MCM-Ti-Au-(2%)(4)

3.2.6 FTIR spectroscopy

Fig.13 shows FTIR spectra of MCM-Ti , MCM-Ti-Au (2%) as-synthesized and MCM-Ti-Au (2%), MCM-Ti-Cr (2%) calcined at 773K samples. The bands at 623 and 569 cm-1in MCM-Ti-Cr (2%) are found to be due to extra framework chromium oxide as reported earlier [66].The peaks near 1089 and 802 cm^{-1} correspond to asymmetric and symmetric vibrations of Si-O-Si linkage respectively. The peak at 464 cm^{-1} has been ascribed to bending vibration of Si-O-Si linkage. The band at 952 cm^{-1} can be assigned to Si-O-Ti vibration which is also assigned to lattice defect and is correlated to the presence

of Cr as well as Ti ions [67].This absorption band is absent in calcined MCM-Ti-Au (2%) sample containing gold.

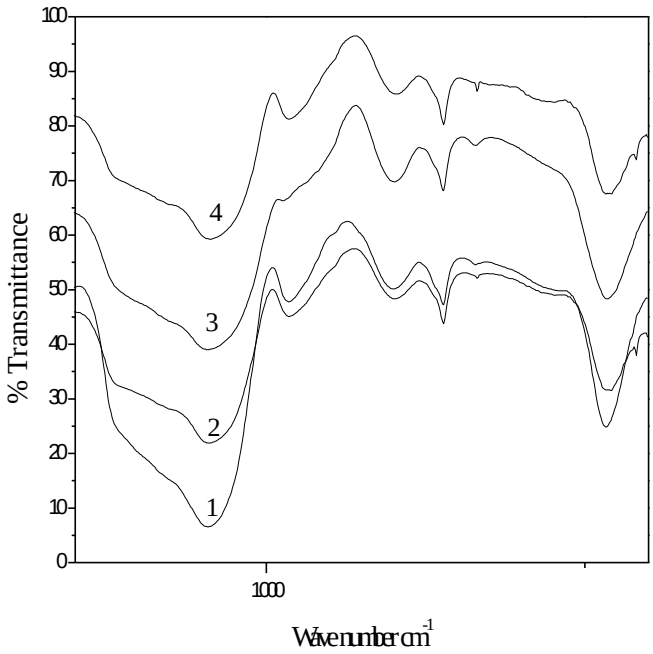

Fig.13 : FTIR spectra of MCM-Ti (1), MCM-Ti-Au (2%) as-synthesized (2), MCM-Ti-Au (2%) (3) and MCM-Ti-Cr (2%) (4).

3.2.7 Energy Dispersive Spectrometer (EDS)

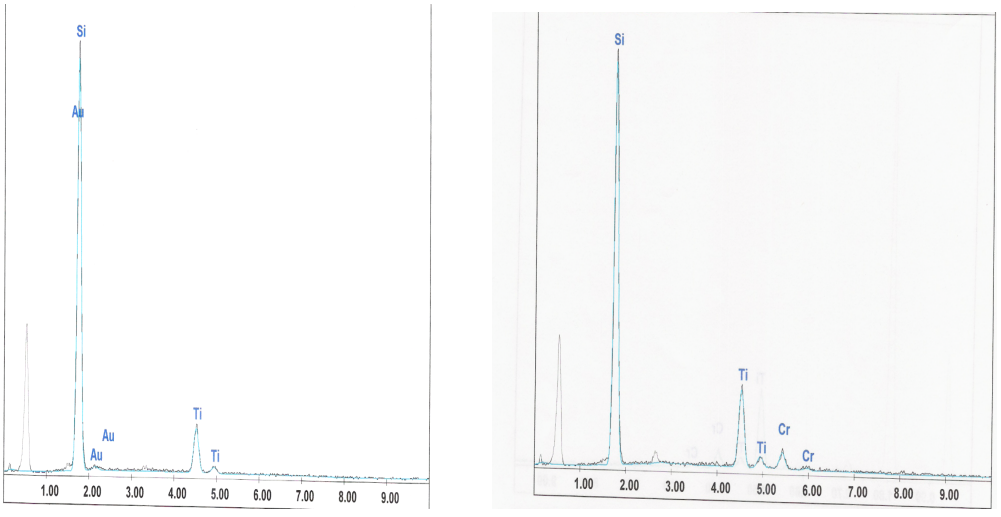

Fig. 14 EDS of [A] MCM-Ti-Au and [B] MCM-Ti-Cr

Fig. 14 shows elemental analysis of MCM-Ti-Au (2%) and MCM-Ti-Cr (2%).
The presence of Au or Cr along with Si and Ti can be seen from EDS spectrum. This is a semiquantitave nondestructive technique.

3.3. Catalytic activity measurements

Various characterization techniques reveal that titanium, gold and chromium are present on the surface of MCM-41 and hence the materials were tried for oxidation of acetone. The degradation of acetone was studied at different concentrations under UV radiation.

3.3.1 Catalytic Activity on MCM-Ti-Au (2%)

Curves (1-3) in Fig.15 show the yield of CO_2 as a function of radiation dose, when a mixture of acetone + air, containing varying concentration of acetone, was reacted over

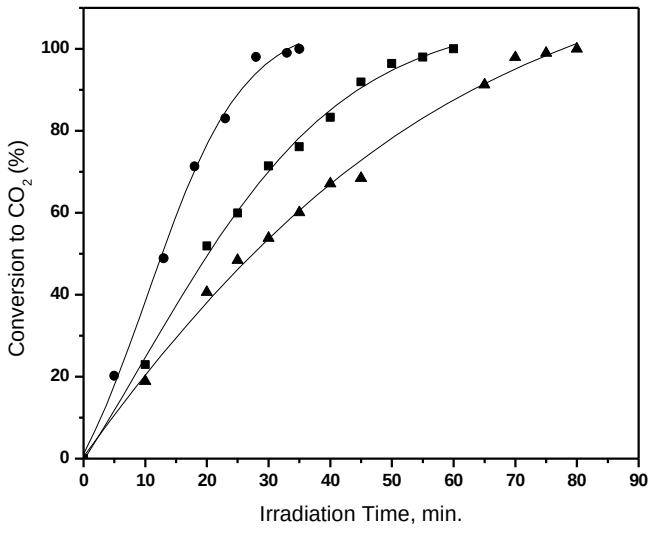

Fig.15 Yield of CO_2 (curves 1-3) as a function of time, when MCM-Ti-Au (2%) was used for the UV-induced vapor-phase photo-catalytic oxidation of acetone present at varying concentrations in air. Curve 1) 1.47, 2) 2.01, 3)3.7 mol%.

MCM-Ti-Au (2%) calcined at 623 K. As seen in the results of curves (1-3) in Fig. 13, the rate of the reaction depended upon acetone concentration, the lower the concentration the faster being the reaction. During this experiment, 100% conversion to CO_2 was observed for acetone concentration of 1.47 , 2.01 and 3.7 µmoles % acetone in air and the values of $t_{1/2}$ (time taken for 50% conversion of acetone) being 10, 15 and 19 minutes respectively.. It was observed that calcination of a sample at higher temperatures resulted in considerable loss of catalytic activity most probably due to change in the crystallite size.

3.3.2 Catalytic Activity on MCM-Ti-Cr (2%)

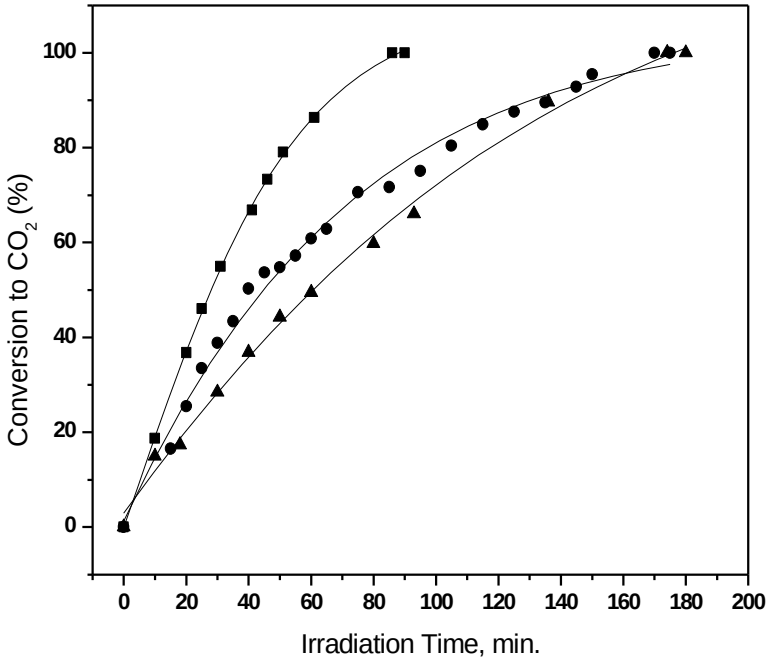

Fig.16 Yield of CO_2 (curves 1-3) as a function of time, when MCM-Ti-Cr (2%) was used for the UV-induced vapor-phase photo-catalytic oxidation of acetone present at varying concentrations in air. Curve 1) 0.968, 2)1.96, 3)4.2 mol%.

Curves (1-3) in Fig.16 show the yield of CO_2 as a function of radiation dose, when a mixture of acetone + air, containing varying concentration of acetone, was reacted over MCM-Ti-Cr (2%) calcined at 623 K. Here the reaction rate is slow as compared to samples containing same amount of gold. The reaction is carried out in a closed reactor

and O_2 concentration goes down leading to increase of electron concentration resulting in the variation in the oxidation state of chromium [68]. However, 100% conversion to CO_2 was observed for acetone concentration of 0.968, 1.96 and 4.2 µmoles % acetone in air the value of $t_{1/2}$ being 38, 50 and 80 minutes respectively. It can be seen that the rate of the reaction depended upon acetone concentration, the lower the concentration the faster being the reaction.

3.3.3 Catalytic Activity on MCM-Ti

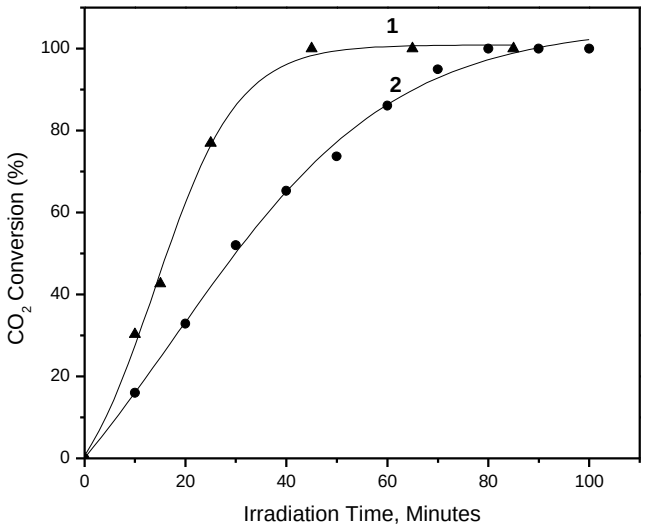

Fig.17 Yield of CO_2 (curves 1-2) as a function of time, when MCM-Ti was used for the UV-induced vapor-phase photo-catalytic oxidation of acetone present at varying concentrations in air. Curve 1) 1.72, 2) 2.78 mol%.

Curves (1-2) in Fig.17 show the yield of CO_2 as a function of radiation dose, when a mixture of acetone + air, containing varying concentration of acetone, was reacted over MCM-Ti calcined at 623 K. Here also in absence of metal it can be seen that the rate of the reaction depended upon acetone concentration, the lower the concentration the faster being the reaction. However, 100% conversion to CO_2 was observed for acetone concentration of 1.72 and 2.78 µmoles % acetone in air, the value of $t_{1/2}$ being 15 and 30

minutes. Here the reaction rate is slow as compared to samples containing gold but it is fast as compared to samples containing Cr.

These results thus provide evidence that the activity of a catalyst is governed by multiple factors. In addition to surface area and gold content, morphology of TiO_2 and the size of the gold particles also contribute significantly to the overall catalytic activity.

It can be seen from the above studies that the time required for complete degradation of acetone is different from sample to sample.MCM-41 helps to get better dispersion of transition metals due to its large surface area. Transition metal is added to increase the life time of the excited electron and the created positive holes and to improve the activity. The activity for degradation of acetone is better of MCM-Ti –Au (2%) than MCM-Ti. Here incorporation of gold helps to increase the life time of the excited electrons and created holes. Thus the time required for complete degradation of acetone with same concentration is less as compared to MCM-Ti. On the other hand the Cr containing samples show less activity as compared to MCM-Ti. The variable oxidation state of chromium is responsible for this decrease in activity.

The role of co-catalyst:

The higher activity in presence of Au as reflected in the $t_{1/2}$ values may be attributed to the adsorption of O_2 molecules over nanosize clusters of Au dispersed in MCM-41. Small size gold crystallites are known to serve as very efficient catalytic sites for oxidation reactions. In case of Cr, since Cr undergoes a valence change on adsorption of O_2 , such promotion of catalytic reaction is not observed. The lower catalytic activity of Cr containing sample may be attributed to lower surface area of MCM-Ti-Cr (2%) as compared to MCM-Ti

3.4 Mechanism of Photocatalysis

The aim of semiconductor photocatalysis is to effectively detoxify organic pollutants. UV or visible light is used to create electron hole pairs in the semiconductor. The electrons then react with oxygen in the sample to form O_2^- and holes react with surface hydroxyl groups to form OH· radicals. The radical species then attack the organic molecule which is eventually oxidized to CO_2 and H_2O. We have studied the photocatalytic oxidation of

acetone in vapour phase. The mechanism of semiconductor photocatalysis is shown below.

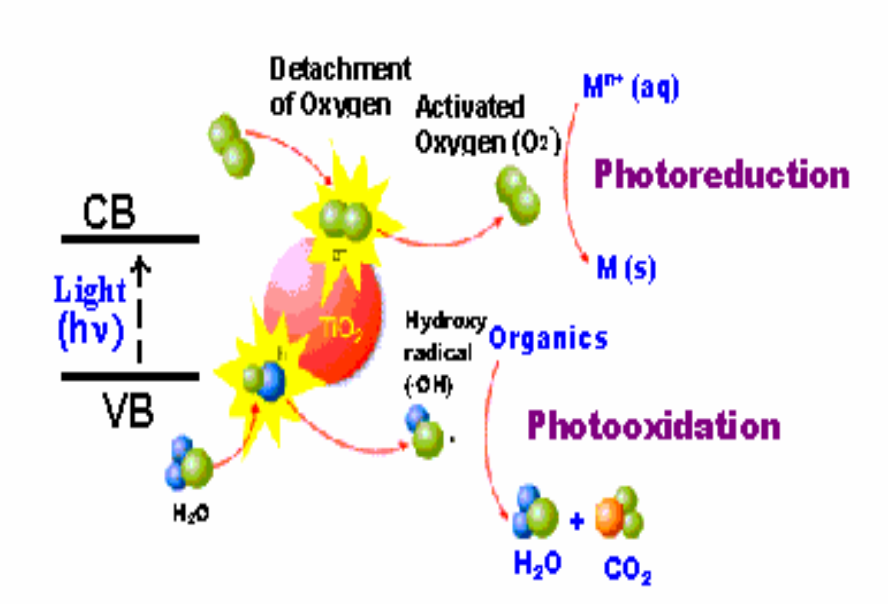

$(TiO_2) + h\nu \rightarrow e^- + p^+$

$O_2 + e^- \rightarrow O_2^-$

$H_2O \leftrightarrow OH^- + H^+$

$O_2^- + H^+ \leftrightarrow HOO^{\cdot}$

$OH^- + p^+ \rightarrow {}^{\cdot}OH$

$R\text{-}H + {}^{\cdot}OH \rightarrow {}^{\cdot}R + H_2O$

$R + HOO^{\cdot} \rightarrow ROOH \rightarrow \text{Intermediate} \rightarrow CO_2$

Fig. 18: Semiconductor Photocatalysis

CONCLUSIONS

1. MCM-Ti-Cr and MCM-Ti-Au samples were prepared keeping Si/Ti mole ratio 10 and doped with about 0-2% metal (Cr or Au) by impregnation method. Samples were characterized using XRD, diffuse reflectance UV-visible, SEM, TEM, low temperature N_2 adsorption and FTIR techniques.

2. Reflection at 2? =25^o, 38$^?$,48^o ,55^o and 63^o for all the samples are due to anatase TiO_2 XRD revealed that the size of crystallites in different samples, as calculated from the width of I_{112} reflection by using Scherrer's equation, is in the range 10-25 nm. The presence of small amount of gold is indicated by a weak and broad XRD line appearing at 44.5^o (d = 2.04 Å) revealing the small size of Au crystallites. Small peaks due to Chromium Oxide are located in the XRD spectrum of MCM-Ti-Cr (2%).

3. Diffuse reflectance UV-vis spectra of MCM-Ti-Cr (2%) show absorption at 450 and 550 nm due to charge transfer and d-d transition respectively. MCM-Ti-Au samples show a band at 250 nm with less intensity for more gold containing sample.

4. The pore size and BET surface area of Cr or Au loaded samples decreases as compared to MCM-Ti samples due to blocking of pores.

5. The band at 952 cm^{-1} can be assigned to Si-O-Ti vibration which is also assigned to lattice defect and is correlated to the presence of Cr as well as Ti ions .This absorption band is absent in calcined MCM-Ti-Au (2%) sample containing gold.

6. TEM pictures show that the particles of MCM-Ti-Au (2%) and MCM-Ti-Cr (2%) are of nano size.

7. No reaction occurred over MCM-Ti and MCM-Ti-Cr [2%] and MCM-Ti-Au [2%] samples, when acetone vapor + air were reacted at room temperature in the presence of

visible light. The reaction products formed during photo-oxidation of acetone under UV-irradiation were mainly carbon dioxide and water. In the case of chromium containing sample, the reaction rate is slow as compared to samples containing same amount of gold. This is due to the variable oxidation state of chromium. The photocatalytic activity results provide evidence that the activity of a catalyst is governed by multiple factors. In addition to surface area and gold content, morphology of TiO_2 and the size of the gold particles also contribute significantly to the overall catalytic activity.

REFERENCES

[1] B. Delmon, Coll, Scientific Bares for the Preparation of Heterogeneous Catalysis, Vol. I- VI, Elsevier, 1980.

[2] K. S. W. Sing, D.H. Everett, R.H.W. Haul, L. Moscou, R.A. Pierotti, J. Rouquerol, T. Siemieniewska, Pure Appl. Chem. 57 (1985) 603.

[3] C. T. Kresge, M. E. Leonowicz, W. J. Roth, J. C. Vartuli, J.S. Beck, Nature 359 (1992) 710.

[4] J. S. Beck, J. C. Vartuli, W. T. Roth, M. E. Leonowicz, C. T. Kresge, K. D. Schmitt, C. T. W. Chu, D. H. Olson, E. W. Sheppard, S. B. Mc Cullen, J. B. Higgins, J. L. Schlenker, J. Am. Chem. Soc. 114 (1992) 10834.

[5] C. J. Brinker, Curr. Opin. Solid State Mater. Sci. 1 (1996) 798

[6] J. C. Vartuli, C. T. Kresge, W. J. Roth, S. B. Mc Cullen, J. S. Beck, K. D. Schmitt, M.E. Leonowicz, J. D. Lutner, E. W. Sheppard, Advanced Catalysts and Nanostructured Materials: Modern Synthesis Methods, Academic Press, New York, 1996.

[7] A. Sayari, Chem. Mater. 8 (1996) 1840.

[8] J. Y. Ying, C. P. Mehnert, S. Wong, Angew. Chem. Int, Ed. 38 (1999) 56.

[9] A. Corma, Chem. Rev. 97 (1997) 2373.

[10] P. A. Winsor, Chem. Rev. 68 (1968) 1.

[11] P. Ekwall, Advances in Liquid Crystals, Ed. G. H. Brown, Academic Press Inc New York, 1971.

[12] J. C. Vartuli, C. T. Kresge, M. E. Leonowicz, A. S. Chu, S. B. Mc Cullen, I. O. Johnson, E. W. Sheppard, Chem. Mater. 6 (1994) 2070

[13] C. Y. Chen, S. L. Burkett, H. X. Li, M. E. Davis, Microporous Mater. 2 (1993) 27.

[14] A. Steel, S. W. Carr, M. W. Anderson, J. Chem. Soc., Chem. Commun. (1994) 1571.

[15] A. Monnier, F. Schuth, Q. Huo, D. Kumar, D. Margolese, R. S. Maxwell, G. D. Stucky, M. Krishnamurthy, P. Petroff, A. Firrouzi, M. Janicke, B. Chmelka, Science 261 (1993) 1299.

[16] G. D. Stucky, A. Monnier, F. Schuth, Q. Huo, D. Margolese, D. Kumar, M. Krishnamurthy, P. Petroff, A. Firouzi, M. Janicke, B. F. Chmelka, Mol. Cryt. Liq. Cryt. 240 (1994) 187.

[17] A. Firouzi, D. Kumar, L. M. Bull, T. Besier, P. Sieger, Q. Huo, S. A. Walker, J. A. Zasadzinski, C. Glinka, J. Nicol, D. Margolese, G. D. Stucky, B. F. Chmelka, Science 267 (1995) 1138.

[18] R. K. Iler, The Chemistry of Silica, Wiley, New York, (1979).

[19] H. P. Lin, C. Y. Mou, J. Cluster Sci. 10 (1999) 271.

[20] H. P. Lin, S. Cheng, C. Y. Mou, J. Chin. Chem. Soc. 43 (1996) 375.

[21] Z. Zhang, Y. Han, L. Zhu, R. Wang, D. Zhao, F. S. Xiao, Angew. Chem. Int. Ed. 14 (2001) 1258

[22] P. J. Bruinsma, A. Y. Kim, J. Liu, S. Baskaran, Chem. Mater. 9 (1997) 2507.

[23] H. Yang, N. Coombs, I. Sokolov, G.A. Ozin, Nature 38 (1996) 589.

[24] L. Davydov, E.P. Reddy, P. France and P.G. Smirniotis, J. Catal. 203 (2001) 157.

[25] H. Yamashita, M. Harada, J. Misaka, M. Takeuchi, B. Neppolian and M. Anpo, Catal. Today 84 (2004) 191.

[26] K.E. Karakitsou and X.E. Verykios, J. Phys. Chem. 97 (1993) 1184.

[27] M. Anpo, Y. Ichihashi, M. Takeuchi and H. Yamashita, Science and technology in Catalysis, 305 (1998) 121.

[28] Q. Sheng, S.Yuan, J.Zhang and F.Chen., Micropor. Mesopor. Mater. 87 (2005) 177.

[29] X. Fu, W.A. Zeltner and M.A. Anderson, Appl. Catalysis B: Environ 6 (1995) 209.

[30] J.Yu, Y.Su, B.Cheng and M. Zhou, J. Mol. Catal. A: Chemical 258 (2006) 104.

[31] A.J. Maira. K.L.Yeung, C.Y.Lee, P.L.Yue and C.K.Chau, J. Catal. 192 (2000) 185.

[32] A. Sirisuk, C.G.Hill Jr, M.A. Anderson, Catal. Today 54 (1999) 159.

[33] K.L.Yeung, S.T.Yau, A.J. Maira, J.M.Coronado, J. Soria and P.L. Yue, J. Catal. 219 (2003) 107.

[34] H. Hayashi and K.Torii, J. Mater. Chem. 12 (2002) 3671.

[35] Y,-F. Chen, C.-Y. Le, M.-Y. Yeng and H.-T. Chiu, Mater. Chem. Phys. 81 (2003) 39.

[36] J.-Y. Zheng, J.-B. Pang, K.-Y. Qiu and Y. Wei, Micropor. Mesopor. Mater. 49 (2001) 189.

[37] JianHong Lee, Ing Chi Leu, Ming Chi Hsu, Yi-Wen Chung and Min Hsiung Hon, J. Phys. Chem. B 109 (2005)13056.

[38] N.Negishi, K.Takenchi, T.Ibusuki, J. Mater. Sci. 33 (1998) 5789.

[39] Y.Tanaka, Ceram. Soc. Jpn. 106 (1998) 344.

[40] M.Anpo, S. Dohshi, M. Kitano, Y.hu, M.Takenchi and M.Matsuoka, Annual rev. Mater. Res. 35 (2005) 1.

[41] M.Anpo, J. Photochem. Photobiol. A 148 (2002) 257.

[42] Ji-Chuan Xu, Yan-Li Shi, Ji-Er Huang, Bo wang and Hu-Lin Li, J.Mol.Catal. A: Chemical 219 (2004) 351.

[43] S. Karvinen, Sol. State Scien. 5 (2003)811.

[44] C.-G Wu, C-C Chao and F-T Kuo, Catal. Today 97 (2004)103.

[45] F.B.Li, X.Z.Li, Appl. Catal. A: Gen. 228 (2002)15.

[46] A. Linsebigler, G. Lu, J.T. Yates, Chem. Rev. 95 (1995) 735.

[47] C.Y. Wang, C.Y. Liu, J. Chen, T. Shen, J. Colloid. Interface Sci. 191 (1997) 464.

[48] C.Y. Wang, C.Y. Liu, X.Zheng, J. Chen, T. Shen, Colloid Surf. A, 131 (1998) 271.

[49] A.Selafani, L. Palmisana, G.Marci and A. Verezia, Sol. Energy Mater. Sol. C, 51(1998) 203.

[50] J.C. Yang, Y.C. Kim, Y.G. Shul, C.H.Shin and T.K.Lee, Appl. Surf. Sci. 121/122 (1997) 525.

[51] W. Choi, A.Termin, M.R. Hoffmann, J. Phys. Chem. 98 (1994) 13669.

[52] K.Bhattacharya, A.K.Tripati, G.K.Dey and N.M.Gupta, J.Nanosci. Nanotech. 5 (2005) 790.

[53] K.Bhattacharya, S.Varma, D.kumar, A.K.Tripati and N.M.Gupta, J. Nanosci. Nanotech. 5 (2005) 797.

[54] L.Davydov, E.P.Reddy, P.France and P.G.Smirniotis, J.Catal. 203 (2001)157.

[55] Y.Xu and C.H.Langford, J. Phys. Chem. B 101 (1997) 3115.

[56] R.Ashai, T.Morikawa, T.Ohwaki, K.Aoki, Y.Taga, Science 293 (2001) 270

[57] G. Hitoki, T. Takata, J.N. Kondo, M. Hara, H. Kobayashi and K. Domen, Chem.

Commun. 16 (2002) 1698.

[58] C.H.Rhee, S.W.Bae and J.S.Lee, Chem. Lett. 34 (2005)660.

[59] A.R. Gandhe, S.P. Naik and J.B. Fernades, Micropor. Mesopor. Mater. (2005) 103.

[60] C.T. Kresge, M.e. Leonowicz, W.J. Roth, J.C. Vartuli and J.S. Beck, Nature 359 (1992)710.

[61] Jian Chen, D.F. Ollis, W.H. Rulkens and H. Bruning, Wat. Res. 33(1999) 661

[62] . S.C. Laha and R. Kumar, Micropor. Mesopor. Mater. 53 (2002)163.
K. Mukhopadhyay, A. Ghosh, R. Kumar, Chem. Commun. (2002) 2404

[63] Z.D. Zhu, Z.X. Chang and L. Kevan, J. Phys. Chem. B 103(1999) 2680

[64] .S. Zheng, L. gao, Q. Zhang and J. Guo, J. Mater. Chem. 10(2000) 723.

[65] M.Kruk, M.Jariniec, Y. Sakamoto, O.Terasaki, R. Ryoo, C.H.Ko, J. Phys. Chem. B 104 (2000) 292.

[66] J.A. Gadsden, Infrared Spectra of Minerals and related Inorganic Compounds, Butterworth and Co. Publishers Ltd. 1975,pp 44.

[67] T. Chapus, A. Tuel, Y. Taarit and C. Naccache, Zeolites 14 (1994) 349.

[68] S.Rodrigues, K.T. Ranjit, S. Uma, I. N. Martyanov and K.J. Klabunde, J. Catal. 230(1) (2005) 158